2014-01-01

E-Quality Control Using 3D Reconstruction and 3D Measurement

Jun Zheng
University of Texas at El Paso, dream63star@gmail.com

E-QUALITY CONTROL USING 3D RECONSTRUCTION AND 3D MEASUREMENT

JUN ZHENG

Department of Industrial Engineering

APPROVED:

_____
Tzu-Liang (Bill) Tseng, Ph.D., Chair

_____
Yirong Lin, Ph.D., Co-Chair

_____
Eric D Smith, Ph.D.

_____
Charles H. Ambler, Ph.D.
Dean of the Graduate School

E-QUALITY CONTROL USING 3D RECONSTRUCTION AND 3D MEASUREMENT

By

JUN ZHENG

THESIS

Presented to the Faculty of the Graduate School of

The University of Texas at El Paso

in Partial Fulfillment

of the Requirements

for the Degree of

MASTER OF SCIENCE

Department of Industrial Engineering

THE UNIVERSITY OF TEXAS AT EL PASO

August 2014

ACKNOWLEDGEMENTS

I express my gratitude to all my family members and friends for their support without which this thesis would not have been possible. I would like to express my sincere thanks to Dr. Tseng for believing in me and choosing me for this research. I would like to thank Dr. Yirong Lin, and Dr. Eric Smith for being my committee members and dedication of their valuable time with this research. I would also like to thank Mr. Luis A. Ochoa from W.M. Keck Center for their valuable support without which this thesis would not have been possible.

ABSTRACT

Recently more and more industrial applications use image acquisition to improve product manufacturing. The observed growth in the last few years is mainly due to the great advances in acquisition devices which are now affordable for more industrialists. Moreover, the increasing demands in the quality requirements of the products are a great stimulus to apply vision tools which allow a better understanding of the impact of the manufacturing process on the product quality. Vision tools have been used in many industrial fields. But the traditional 2D vision is not as reliable as 3D measurement due to the limitations of the technology and the structure of a part. In this study, a novel approach which integrates photometric stereo reconstruction and 3D measurement for classifying the parts into different categories is presented. The data extracted from several case studies demonstrates the proposed methodology. Results show that the new methodology yielded superior results compared to the traditional inspection approaches with very high classification accuracy. Moreover, the proposed approach is capable to archive 3D models of the parts and achieve rapid quality control. This paper forms the basis for solving many other similar problems that occur in many industries.

TABLE OF CONTENTS

LIST OF TABLES

LIST OF FIGURES

Chapter 1

INTRODUCTION

1.1 Background

Nowadays industry faces increased challenges caused by global competition, new technologies and electronic commerce. Companies must to move towards shorter product life cycle, remote quality control, smaller products and network based production and distribution systems to stay in the competition. E-manufacturing [9-16] is the process of integration of design, manufacturing, quality and business functions with integrated information networks. The competition in the manufacturing industry made companies to manufacture high-quality products. In other words, industry is striving towards achieving zero defect manufacturing, which requires the manufacturer to test each and every part produced. In such scenarios, a new paradigm of sensor-based, automated, real-time, internet based inspection systems are proposed to help perform quality inspection reliably, accurately and in very less time (i.e. e-quality). E-quality integrated with the information network, allows a remote quality control with a minimal human intervention. The probability of defective products propagating into the downstream is minimized by embedding various sensors, communications, and fast computing platforms for accurate and timely decision making onto the production lines. Also the inspection data can be reused for the analysis of process capability and distributed to the relevant entities for the initiation of corrective actions.

1.2 E-quality control framework

Figure 1.1 outlines the overall framework for the proposed project. In Phase I, the research effort will be focused on development of Inspection Support System (ISS) using image-based stereo reconstruction and virtual prototyping (i.e., 3D model generation). Basically, the standard part will be used to generate the 6 images from different angles through the Machine Vision System (MVS). After these images have been produced, they will be used to construct the standard 3D model (i.e., virtual prototyping) and the model will be saved in the PC. Later, assuming the in-coming part is delivered, and then it will be through a similar procedure and compared with the standard 3D model. After the comparison is implemented, the contrast and difference between two parts will be identified. Finally, the inspection outcomes will be reported as pass, rework and discard.

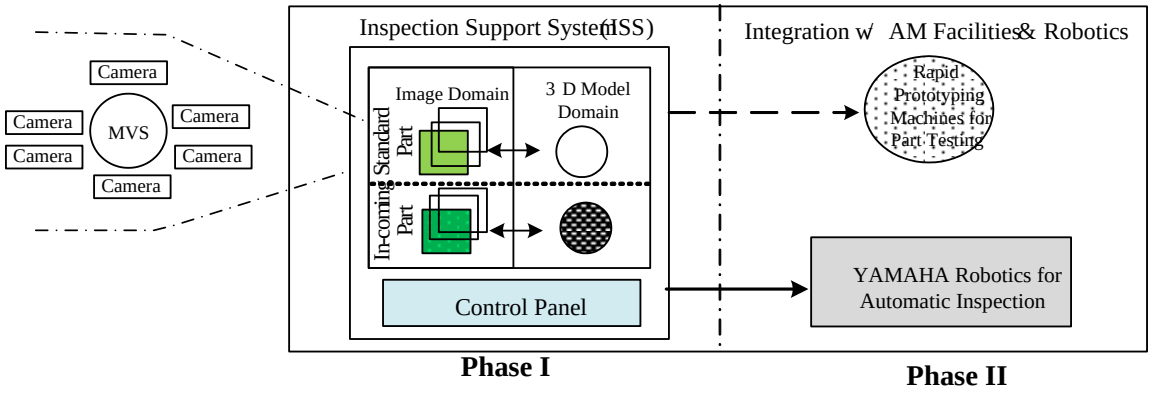

Figure 1.1: The proposed research framework of development of the Remote Quality Control Systems (RQCS)

Figure 1.2 illustrates the integration of ISS with automatic inspection equipment (i.e., YAMAHA robotics) and additive manufacturing facility (i.e., Stratasys FDM 3000 machine). The design of the system is as follows:

1. The Inspection Support System (ISS) will facilitate quality engineers to conduct quality control tasks and identify re-workable parts to reduce expenses. (Phase I)

2. Based on image-based stereo reconstruction and virtual prototyping, the API (Application Programming Interface, a.k.a. GUI) as part of the ISS will help engineers to optimally use machine vision data and the sensor data for part inspection. (Phase I)

3. Integrating ISS with YAMAHA SCARA robotic systems and Stratasys FDM 3000 rapid prototype machine will perform fully automatic inspection through the Remote Quality Control Systems (RQCS). Particularly, the system is anticipated to process data from different sensors through incorporation of the data fusion technique. (Phase II)

4. The RQCS will perform quality control based on functionalities like dimension accuracy, surface roughness/geometry, texture detection, etc…Moreover, this exploration could also include feasibility of inspecting Work-in-Process (WIP) difficult to be dis-assembled.

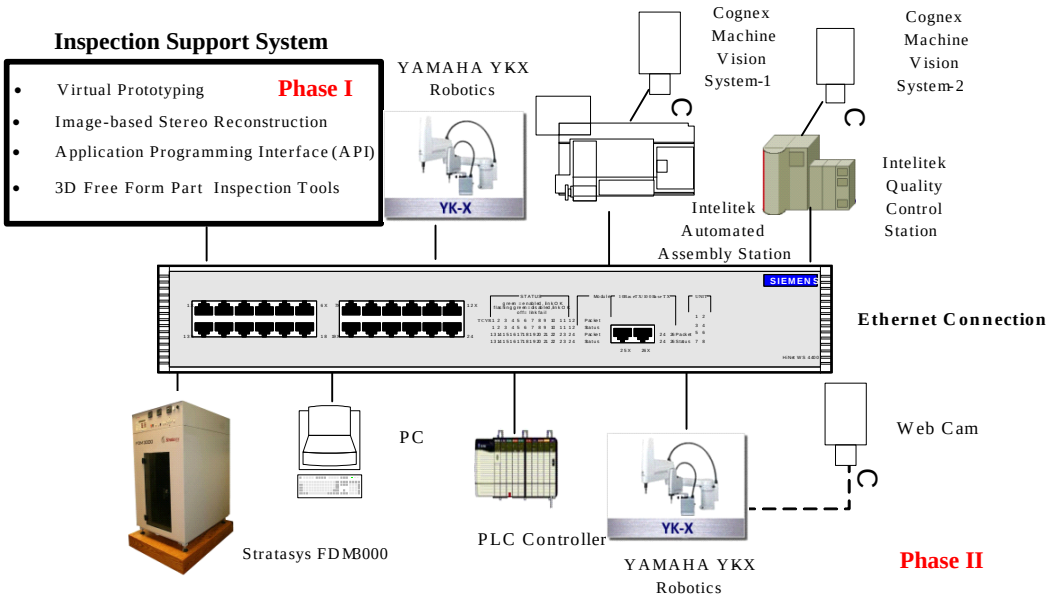

Figure 1.2: Integration of ISS with YAMAHA robotics and Stratasys FDM 3000 machine.

1.3 Motivation of the research

This research proposes a novel 3D E-quality control system that integrates photometric stereo reconstruction for classifying the parts into different categories. The 3D quality control system offers rapid quality control inspection of complex parts. The non-contact photometric scanner provides documented proof that manufacturers are meeting specifications by providing traceable data and accurate 3D models of complex parts, castings, stampings and more. And, the system is very easy to use. The 3D quality control system captures millions of data points in just minutes to represent the true and full geometry of the complex part. The systems then compare the scanned 3D models of produced parts to scanned 3D models of standard parts using 3D measurement based on Kd-tree registration, Hausdorff distance and color mapping to provide accurate and timely measurement feedback for quality control, helping provide proof that the produced products meet the required specification. The data extracted from solar panels and

brake caliper was used as case study to demonstrate the proposed methodology. Results show that the new methodology yielded superior results compared to the traditional inspection approach with very high classification accuracy. Moreover, the proposed approach is capable to archive 3D models of the parts and achieve rapid quality control. This paper forms the basis for solving many other similar problems that occur in many industries.

Chapter 2

LITERATURE REVIEW

2.1 E-quality control

The traditional way of achieving and ensuring the quality standards is mainly via statistical process control (SPC) procedures [23]. However, in sequential manufacturing processes, product quality is influenced by many factors that involve causal relationship and interact with each other. Thus, it is very difficult to set up the best conditions of manufacturing specifications for SPC by executing the design of experiments (DOE) in plants that have large equipment or sequential processes [24]. The conventional SPC and six sigma techniques must respect several statistical assumptions such as normality of distribution of the variables, constant variance of the variables, etc. It is hard to meet all these assumptions in practice.

Current statistical approaches are difficult in analyzing qualitative information such as character the qualitative variable in several levels; and the uncertainty (i.e., variation) of vague observations is essentially non-statistical in nature, and hence these observations may not adequately support the random variation assumption inherent in statistical quality control methods. Moreover, the final solutions derived from standard statistical techniques may not be optimal because these methodologies are not able to learn from historical data. Based on the aforementioned deficiencies from current statistical approaches, a hybrid data mining approach which integrates rough set theory, fuzzy set theory, genetic algorithm and agent based technology is proposed. Comparing to standard statistical tools that use population based approach, the RST uses an individual, object-model based approach that makes a very good tool

for analyzing quality control problems [25]. Furthermore, FST has demonstrated its ability in a number of applications, especially for the control of complex non-linear systems that may be difficult to model analytically. The Genetic Algorithm (GA) operates on a population solution rather than a single solution [26]. To resolve the drawbacks of these statistical methodologies in quality control, the proposed approach expects to provide a way to optimize prediction for the lowest defective rate.

2.2 Photometric stereo reconstruction

Photometric stereo reconstruction computes geographic surface using a fixed viewpoint observations under point lighting, assuming that the object is built with Lambertian material [17]. However, materials usually are not exactly Lambertian, therefore the estimated surface normal is inaccurate. As a result photometric stereo reconstruction has been extended to non-Lambertian materials, which can handle a wider range of material types. But they still rely on isotropic analytical BRDF models that limit their generality [18].

To solve this problem, several approaches have been proposed that not using parametric BRDF models. Hertzmann and Seitz [19] estimate surface normals using a reference object similar material. This method doesn't rely on BRDF models, but it needs a reference object which is not available sometimes. Mallick et al. [20] transfer a general material to Lambertian material by removing the specular component, and then use the traditional photometric stereo reconstruction technique to obtain the surface normals. Other methods make use of general properties of surface reflectance to infer surface statistics. Zickler et al. [21] use Helmholtz reciprocity to recover depth and normal directions. Alldrin and Kriegman [22] utilize the symmetry about the view-normal plane in isotropic BRDF models. Lim and etc. [30] explore the possibility of using

photometric stereo with images from multiple views, when correspondence between views is not initially known. A depth-map with respect to a view, picked from an arbitrary viewpoint as a reference image, serves as correspondences between frames. They compute the depth-map from a Delaunay triangulation of sparse 3D features located on the surface. The they run a photometric stereo computation obtaining normal directions for each depth-map location which is integrated into the resulting depth-map to make it closer to the true surface than the original. Their appraoch presents high quality reconstructions and gives a theoretical argument justifying the convergence of the algorithm. Bernardini and etc. [31] combine the photometric stereo information with the 3D range scan data. The photometric information is simply used as a normal map texture for visualisation purposes. Nehab and etc. [32] produce a very good initial approximation to teh object surface using range scanning technoloty. Normal maps are estimated and then integrated to produce an improved, almost noiseless surface geometry.

2.3 Solar Panels

The solar energy conversion into electricity takes place in a semiconductor device that is called a solar cell. A solar cell is a unit that delivers only a certain amount of electrical power. In order to use solar electricity for practical devices, which require a particular voltage or current for their operation, a number of solar cells have to be connected together to form a solar panel, also called a PV module. For large-scale generation of solar electricity the solar panels are connected together into a solar array [27].

The solar panels are only a part of a complete PV solar system. Solar modules are the heart of the system and are usually called the power generators. One must have also mounting structures to

which PV modules are fixed and directed towards the sun. For PV systems that have to operate at night or during the period of bad weather the storage of energy are required, the batteries for electricity storage are needed. The output of a PV module depends on sunlight intensity and cell temperature; therefore components that condition the DC (direct current) output and deliver it to batteries, grid, and/or load are required for a smooth operation of the PV system. These components are referred to as charge regulators. For applications requiring AC (alternating current) the DC/AC inverters are implemented in PV systems. These additional components form that part of a PV system that is called balance of system (BOS). Finally, the household appliances, such as radio or TV set, lights and equipment being powered by the PV solar system are called electrical load [27].

As we know, a solar panel is an array of solar cells. A solar cell is basically made of pure silicon. The silicon dioxide that can be either quartzite gravel or crushed quartz is first placed into an electric arc furnace. In the electric arc furnace a carbon arc is applied to release the oxygen. The products are carbon dioxide and molten silicon, but at this point, the silicon is still not pure enough in order to be used for solar cells. It requires further purification. Pure silicon is derived from silicon dioxides as quartzite gravel or crushed quartz. Then, the pure silicon is treated with phosphorous and boron in order to produce an excess of electrons and a deficiency of electrons to make a semiconductor capable of conducting electricity. After that, since the silicon disks are shiny, it requires an antireflective coating that is usually titanium dioxide [28].

The cell can be considered as a two terminal device, which conducts like a diode in the dark and generates a photovoltage when charged by the sun. Usually it is a thin slice of semiconductor material of around 100 cm2 in area. The surface is treated to reflect as little visible light as possible and appears dark blue or black [29].

When charged by the sun, this basic unit generates a dc photovoltage of 0.5 to 1 volt and, in short circuit, a photocurrent of some tens of milliamps per cm2. Although the current is reasonable, the voltage is too small for most applications. To produce useful dc voltages, the cells are connected together in series and encapsulated into modules. A module typically contains 28 to 36 cells in series, to generate a dc output voltage of 12 V in standard illumination conditions. The 12 V modules can be used singly, or connected in parallel and series into an array with a larger current and voltage output, according to the power demanded by the application [29].

In this research, we studied efficiency of two types of solar cells: Monocrystalline silicon solar cells and Polycrystalline silicon solar cells. Monocrystalline silicon solar cells are the most efficient type of solar panels. In other words, when sunlight hits these cells, more energy turns into electricity than the other types. As a result of their high silicon content, they're also more expensive. Polycrystalline silicon solar cells have lower silicon levels than Monocrystalline silicon cells. In general, that makes them less expensive to produce, but they're also slightly less efficient.

2.4 Plastic injection

Plastic injection is a manufacturing process in which a thermoplastic is melted and injected by pressure into a mold cavity, cooling down and getting the shape of the mold cavity. Plastic injection has become a very useful technology for various industries like automotive, aerospace, and others. Molds are created with metal materials, usually either steel or aluminum, depending on material properties and specifications. When designing a part for plastic injection, it must be very carefully engineered to facilitate the injection and de-molding process. Part small and

delicate features, material of the mold, material to be injected, capacity of the molding machine, are some of the important points to take into account when using this process.

When a part is manufactured this way, there are several defects that may come up during the process. Depending on the defect, the part may not meet its requirements and may not function as it was intended for. There may be little details easily fixable, but there may be other that will not work at all.

Some of the cosmetic defects may include bubbles, cracking, discoloration, flashing, gouge, haze, scratching, among others. A more complete list of defects and definitions are presented as follows:

- Bubbles
    - Void pockets, typically seen only in transparent parts. may appear as a bulge or protrusion in an opaque part.
- Cracking
    - Stress induced splitting or fissures causing separation of material.
- Discoloration
    - Any change from the original color standard. unintended, inconsistent color.
- Flash
    - Excess plastic at parting line or mating surface of the mold
    - Normally very thin and flat protrusion of plastic along an edge of a part

    - Can also appear as a very thin string or thread of plastic away from the edge of a part.
    - Often found at vents, knock outs and other shut-off areas.
- Gouge
    - Surface imperfection due to an abrasion that removes small amounts of material
    - Depth is measurable.
    - Haze
    - Cloudiness on an otherwise transparent part
- Scratch
    - Surface imperfection due to abrasion that removes small amounts of material.
    - Depth is not measurable.
    - Differs from scratch in mold which leaves a consistent mark.
- Shorts (short shot, non-fill)
    - Missing plastic due to incomplete filling of the mold cavity.
    - Parts are not completely formed.
    - Can usually be identified by smooth, shiny and rounded surfaces.
- Sink

    - Surface depression caused by non uniform material solidification and shrinkage.
    - Most often noted at interface between differing wall thicknesses.
- Specks
    - Small discolored points of matter embedded in the surface.
    - Typically black, caused by material contamination or material degradation
- Splay
    - Off colored streaking.
    - Usually appears silver-like.
    - Splay is caused by moisture in the material or thermal degradation of the resin during processing.
    - A similar look can be caused by cold material skipping across the surface during a fast fill.
    - This is commonly called “jetting”.
- Weld lines
    - Witness line where 2 or more fronts of molten plastic converge.
    - Also called knit lines or flow lines.

Chapter 3

METHODOLOGY

The 3D E-quality control system advances the basic research to address the aforementioned issues through the use of integration of cyber communication, virtual prototyping, photometric stereo reconstruction, robots, and machine vision system. The hardware consists of the state-of-the-art Cognex machine vision systems, YAMAHA robotics systems, and the photometric 3D scanning system in the Intelligent Systems Engineering Lab (ISEL). These equipments and systems provide the foundation for this project. The software consists of Intelligent Graphical User Interface (i.e., Application Program Interface) embedded with photometric stereo reconstruction and data mining algorithms.

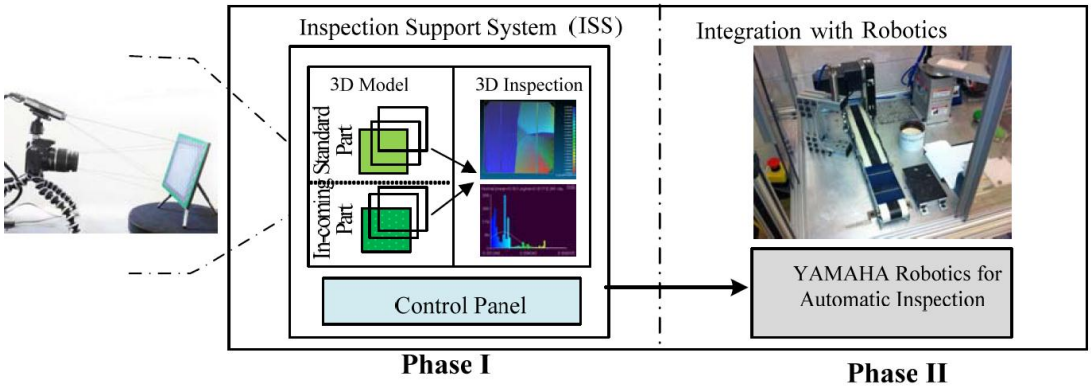

Figure 3.1: The framework of the 3D e-Quality Control Systems (eQCSs)

Figure 3.1 outlines the overall framework for the 3D E-Quality Control Systems. In Phase I, the Inspection Support System (ISS) uses photometric stereo reconstruction to generate the high-resolution 2D images and accurate 3D models for inspection. The 3D scanning System based on the photometric stereo reconstruction is used to capture the high-resolution 2D images of the part

from different angle with several light patterns. After these images have been produced, they are used to construct accurate 3D models which will be saved in the PC and compared with the standard 3D model later for the comparison is implemented, the contrast and difference between two parts will be identified. Finally, the inspection outcomes will be reported as Pass, Rework and Discard. In Phase II, the ISS is integrated with automatic inspection equipment (i.e., YAMAHA robotics) to perform fully automatic inspection through the Remote Quality Control Systems (RQCS). This paper focuses on phase I of the procedure mainly.

3.1 Photometric Stereo Reconstruction

To generate the accurate 3D model for inspection, the 3D scanning system uses photometric stereo reconstruction which uses a SLR camera plus a projector for scanning (see Figure 3.2, 3.6). The projector projects a sequence of four colored strip patterns and one uniform white pattern. In capturing, we take 8 photos for each gradient pattern under two linear polarization states, and 5 stereo photos for each structures light strip patterns, using Cannon 5D cameras in burst mode which requires just a few seconds to capture data at 12 megapixel resolution [20]. Because of noise and the limited resolution of the projector, the structured light scan introduces some high frequencies biasing and noise. We have to smooth the structured light scan surface using bilateral denoising, and then create a surface normal map from the smoothed mesh and extract the high frequency details of the estimated normals using high-pass filtering [20] (see Figure 3.3).

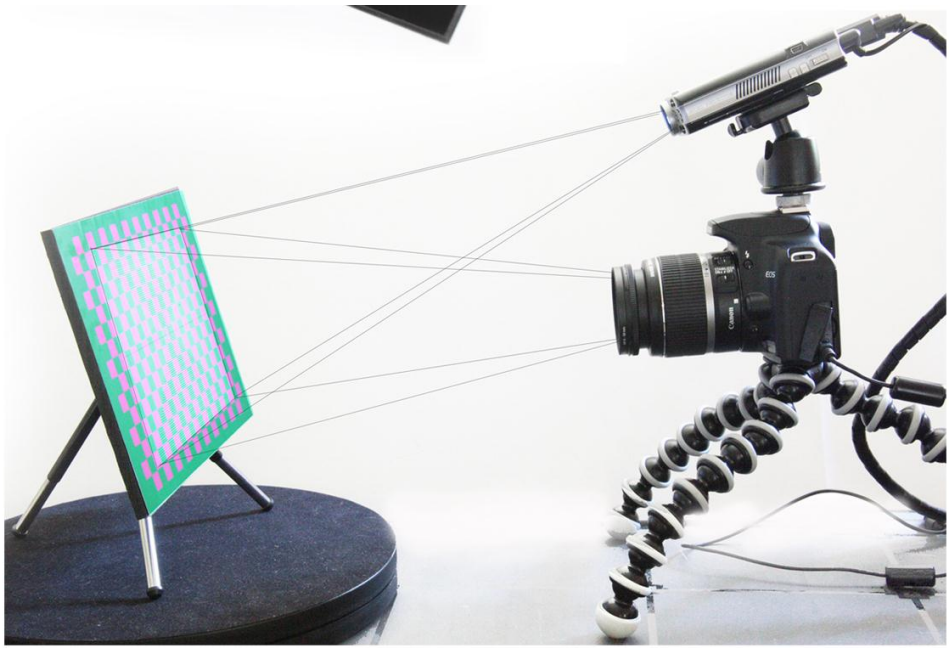

Figure 3.2: The structured-light stereo uses a SLR cameras plus a projector

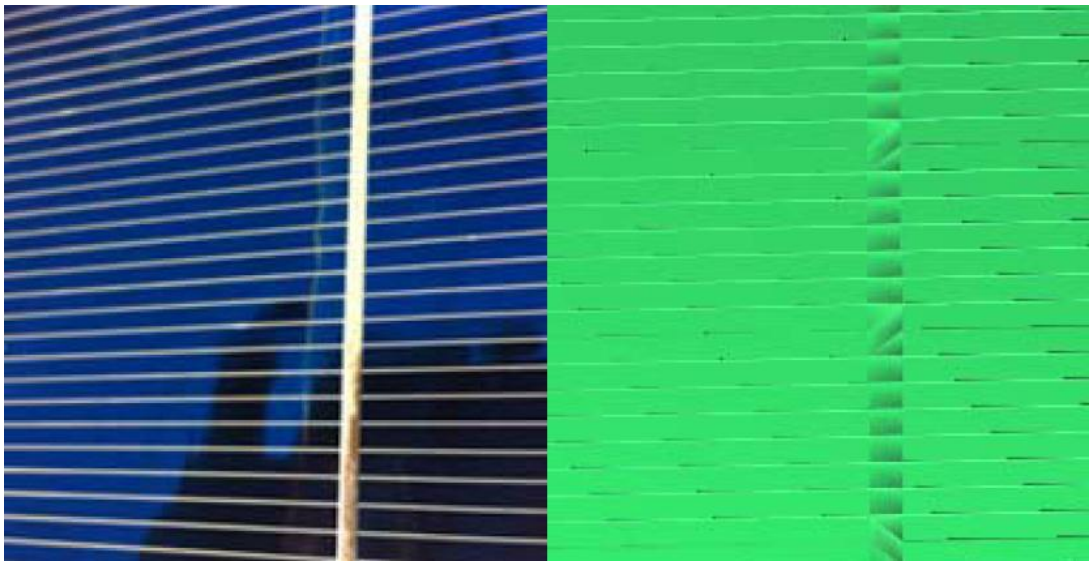

Figure 3.3: Scanned geometry and a real photo of the solar cell

Finally, we optimize the mesh vertices to match this assembled normal map using an embossing process as in [21]. We obtain diffuse and specular normals from gradient illumination for objects

whose reflectance is either diffuse or specular. For polarized patterns, individual linear polarizers are placed over each light. A linear polarizers is mounted on a servomotor in front the camera, which enable to polarizer to be rapidly flipped on its diagonal between horizontal and vertical orientations [20] (see Figure 3.4, 3.5).

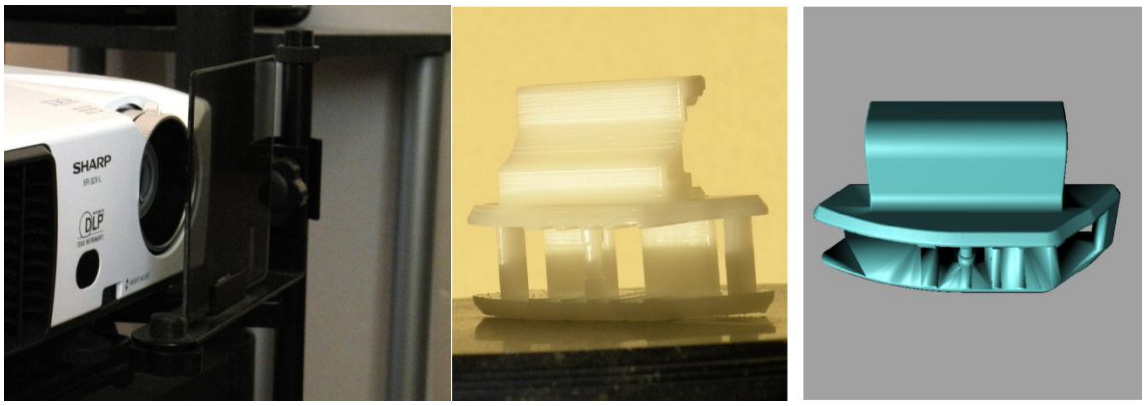

Figure 3.4: Polarizer, a real photo of an object for comparison, and scanned object geometry

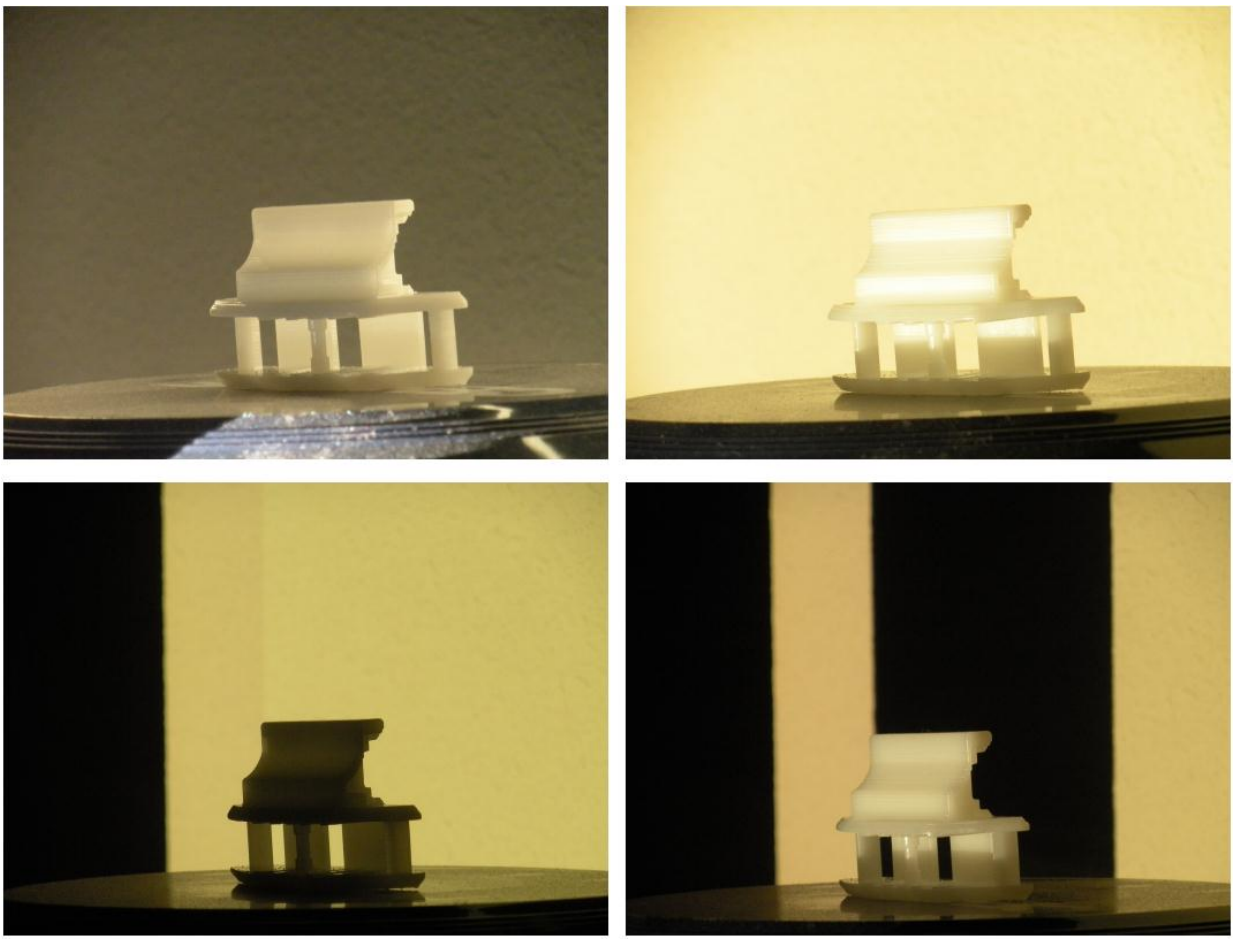

Figure 3.5: Diffuse and specular normals are obtained from gradient illumination for an object whose reflectance is either diffuse or specular

While using normals to improve geometry, we find the measured positions from a range-image. The pixel coordinates on the reference camera induce a natural parameterization of the corresponding surface. Accordingly, under perspective projection, the coordinates of a surface point can be written in terms of a depth function Z(x, y). In other words, given the pixel coordinates, the position of the corresponding surface point P(x, y) has only one degree of freedom, Z(x, y):

$$\boldsymbol{P(x,y)} = \left[-\frac{\boldsymbol{x}}{\boldsymbol{f_x}}\boldsymbol{Z(x,y)}, -\frac{\boldsymbol{y}}{\boldsymbol{f_y}}\boldsymbol{Z(x,y)}, -\frac{\boldsymbol{x}}{\boldsymbol{f_x}}\boldsymbol{Z(x,y)}\right]^{\boldsymbol{T}}$$

where f_x and f_y are the camera focal lengths in pixels. Our problem is to find a depth function that conforms to the estimates we have for the position and normal of each point. To do so, we choose the depth function that minimizes the sum of two error terms: the position error E^p and the normal error E^n.

The position error is then defined as the sum of squared distances between the optimized positions and the measured positions:

$$\left|\left|\boldsymbol{P_i} - \boldsymbol{P_j^m}\right|\right|^{\boldsymbol{2}} = \boldsymbol{\mu_i^2}(\boldsymbol{Z_i} - \boldsymbol{Z_i^m})^{\boldsymbol{2}}, \boldsymbol{where}\ \boldsymbol{\mu_i^2} = (\frac{\boldsymbol{x_i}}{\boldsymbol{f_x}})^{\boldsymbol{2}} + (\frac{\boldsymbol{y_i}}{\boldsymbol{f_y}})^{\boldsymbol{2}} + \boldsymbol{1}$$

Recall that the surface tangents T_x and T_y at a given pixel can be written as linear functions of the depth values and their partial derivatives:

$$\boldsymbol{T_x} = \frac{\boldsymbol{\partial P}}{\boldsymbol{\partial x}} = \left[-\frac{\boldsymbol{1}}{\boldsymbol{f_x}}\left(\boldsymbol{x}\frac{\boldsymbol{\partial Z}}{\boldsymbol{\partial x}} + \boldsymbol{Z}\right), -\frac{\boldsymbol{1}}{\boldsymbol{f_x}}\boldsymbol{y}\frac{\boldsymbol{\partial Z}}{\boldsymbol{\partial x}}, \frac{\boldsymbol{\partial Z}}{\boldsymbol{\partial x}}\right]^{\boldsymbol{T}}$$

$$\boldsymbol{T_y = \frac{\partial P}{\partial y} = \left[-\frac{1}{f_x} x \frac{\partial Z}{\partial y}, -\frac{1}{f_y}\left(y \frac{\partial Z}{\partial y} + Z \right), \frac{\partial Z}{\partial y} \right]^T}$$

Then the normal error is defined as

$$\boldsymbol{E^n = \sum_i [T_x(P_i) \cdot N_i^c]^2 + \left[T_y(P_i) \cdot N_i^c\right]^2}$$

The optimal surface is then given by

$$\boldsymbol{\arg\min_Z \gamma E^p + (1-\gamma) E^n}$$

where the parameter $\gamma \in [0,1]$ controls how much influence the positions and normals have in the optimization. The two error terms are measured in units of squared distance and therefore l is dimensionless. Note that Figure 3.4 depicts the flow chart of photometric stereo reconstruction.

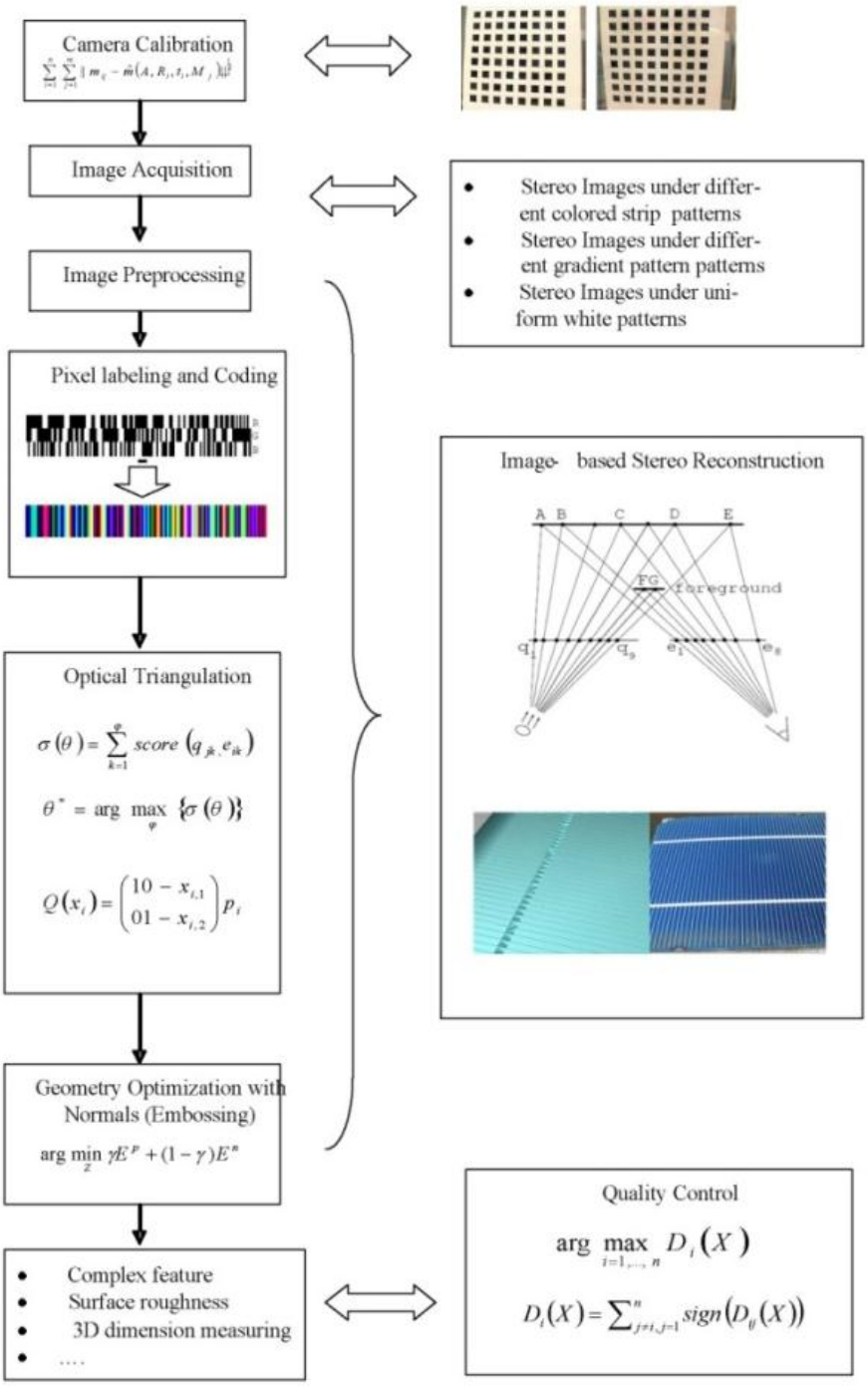

Figure 3.6: The flow chart of photometric stereo reconstruction

3.1.1 Calibration of the scanner

Camera calibration describes the process of the determination of the intrinsic and extrinsic parameters (including lens distortion parameters) of an optical system. Different principles have been applied in order to conduct camera calibration. The choice of the method depends on the kind of the optical system, the exterior conditions, and the desired measurement quality. In case of the calibration of photogrammetric stereo camera pairs, the intrinsic parameters (principal length, principal point, and distortion description) of both cameras should be determined as well as the relative orientation between the cameras.

The position of the camera in the 3D coordinate system is described by the position of the projection center O = (X, Y, Z) and a rotation matrix R obtained from the three orientation angles α, β, and γ. Considering stereo camera systems, only the relative orientation between the two cameras is considered, because the absolute position of the stereo sensor is usually out of interest. In this work, six different angled image pairs are acquired to calibrate the projector and camera for 3D scanning (see Figure 3.7, 3.8).

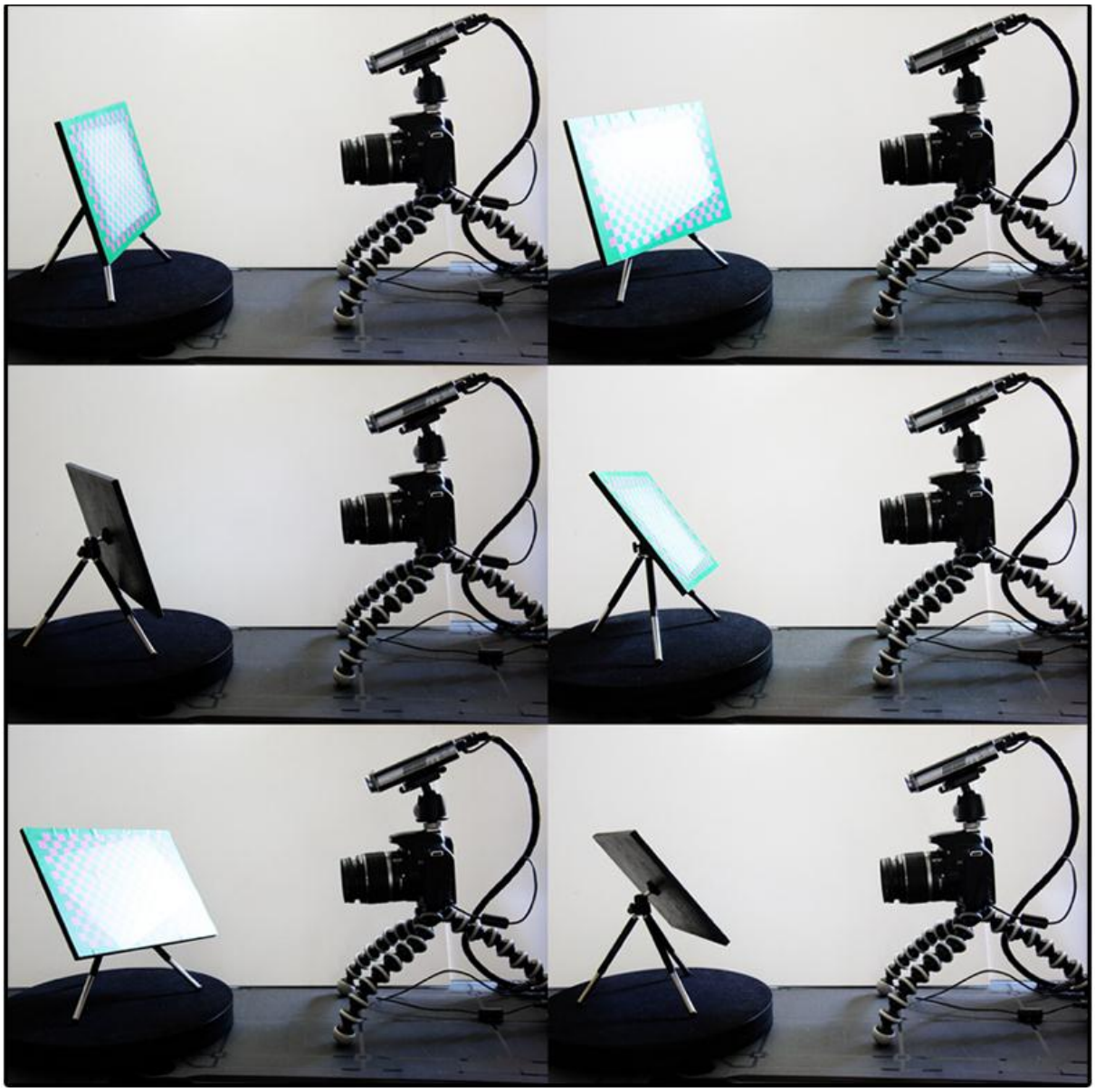

Figure 3.7: Six different angled image pairs are acquired to calibrate the projector and camera for 3D scanning

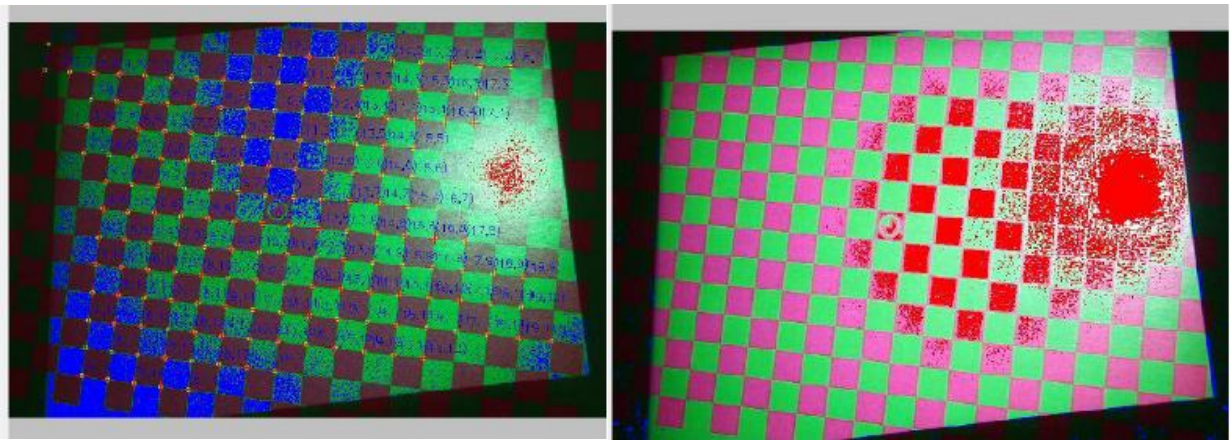

Figure 3.8: Example of good calibration images

3.1.2 Gray code encoding

The method adopts black-white Gray code encoding pattern. In course of decoding, it is different to decoding by pixel centre that the method locates stripe edge in each intensity image (before binarization) by sub-pixel location technology, then adopts points in edge as image sampling points whose grey values (0 or 1) in intensity image (after binarization) are used to acquire Gray code. Gray code value is used to determine the corresponding relationship between edge in intensity image and encoding pattern, and acquire its projecting angle (see Figure 3.9, 3.10).

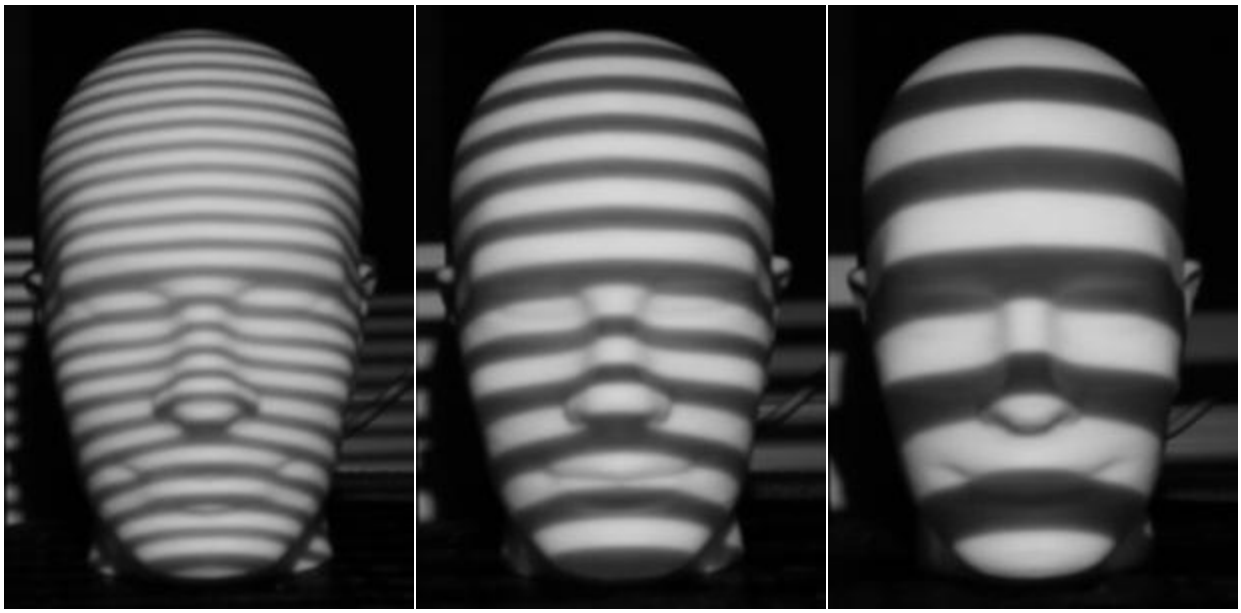

Figure 3.9: Example of gray code encoding

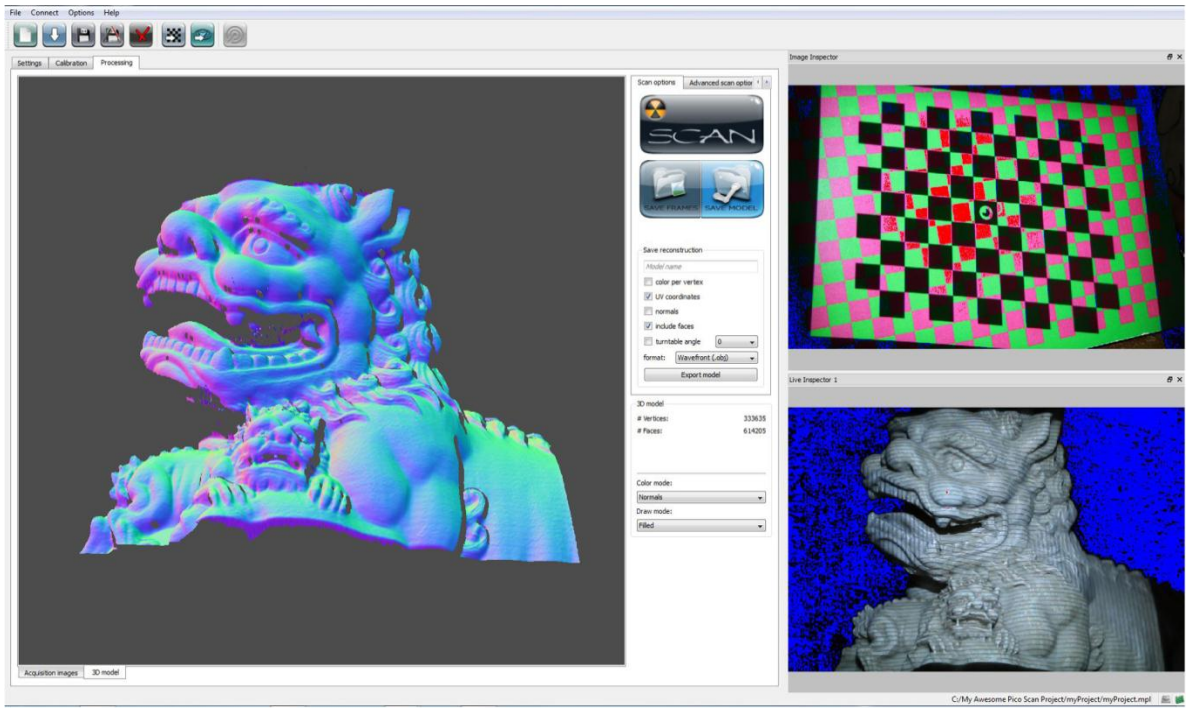

Figure 3.10: 3D reconstruction using gray code.

3.2 The Application Programming Interface (API)

The implementation of remote access can be achieved through the Application Programming Interface (API). The objective of the API development is to provide a Graphical User Interface (GUI) to allow the user to establish and control communication lines with Web-enabled equipment, for example the RP machine remotely. Therefore, the API allows the user to view or measure or operate the part through Machine Vision Systems (MVS), a Web camera and "remote desktop" provided by Microsoft Windows. The 3D quality control API performs 3D inspection using point clouds to measure geometric elements like plane, cylinder, circle, sphere, boundaries, and so on. It extracts features directly from point clouds and gives feedbacks like standard deviation (average error), tolerance and distribution. Also it gets color mapping from surfaces or contours comparison and label edition on particular points for inspection. The inspector then can classify the part into Pass or Fail categories. The 2D Images button can show the inspector the high-resolution images taken during the scanning process that are used to generate the accurate 3D model. The 2D inspection button can also lead the inspector to the Machine Vision System (MVS) for traditional 2D inspection (see Figure 3.11).

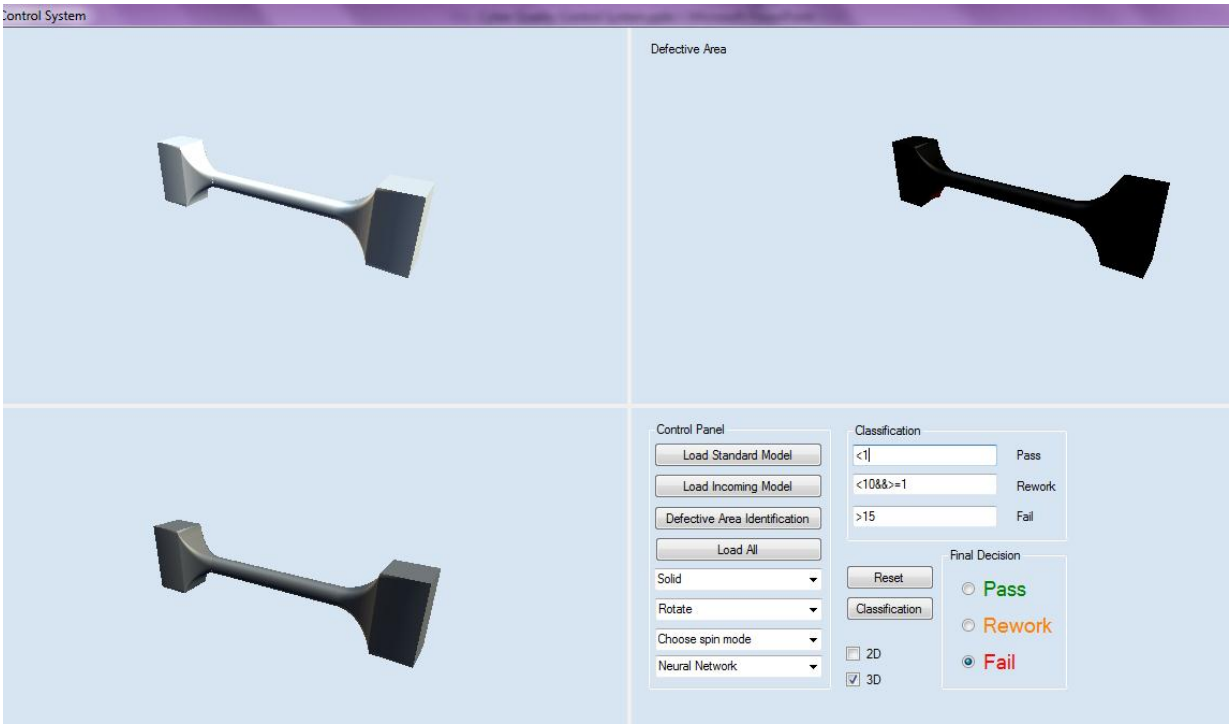

Figure 3.11: 3D Quality Control API

3.3 Quality Control using 3D Measurement

Prior implementing 3D measurement, it is required to register the two models to be compared. The first step is to scale the two models to make sure they are expressed in the same units. First, choose an accurate element, visible in the two models, such as edge, cornice, line or every other rectilinear element. Then, measure the distance, D_{max} between the two specific points in the model with the larger scale, and repeat the process in the other model and get the corresponding distance D_{min}. Eventually, compute the scaling factor $S_f=D_{max}/D_{min}$ and apply it in the smaller model in the f_x, f_y and f_z fields of modify tool of the 3D measurement API. In the second step, we roughly register the two models with translate and rotation tool of the API, and then use the Iterative Closest Point (ICP) algorithm to precisely register and finish the superimposition of the two models (Figure 3.12, 3.13, 3.14).

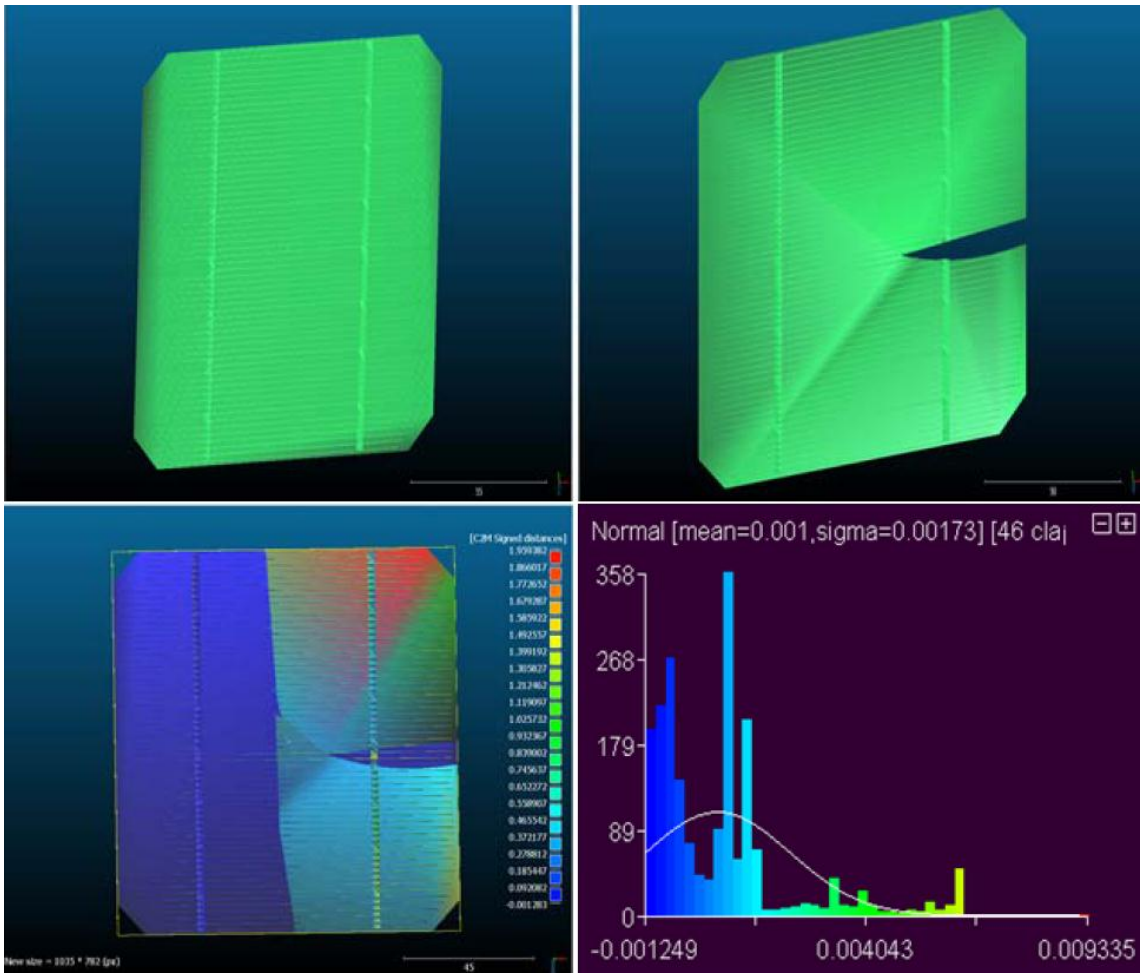

Figure 3.12: The 3D Measurement API snapshot

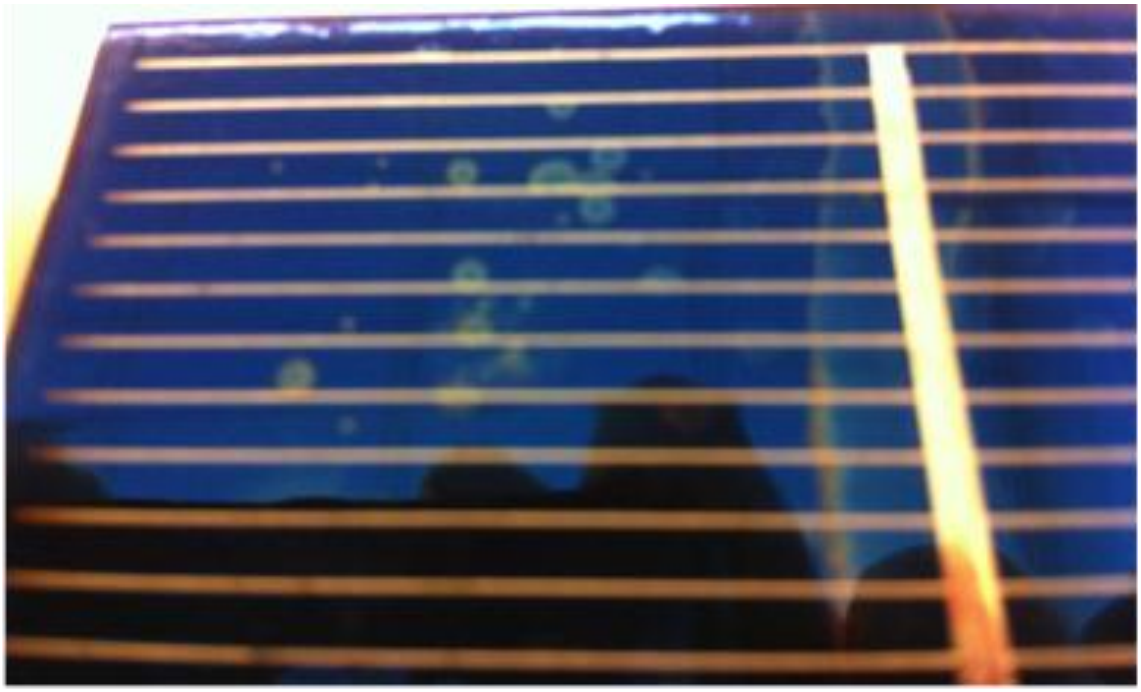

Figure 3.13: Detailed view of the solar cell defects

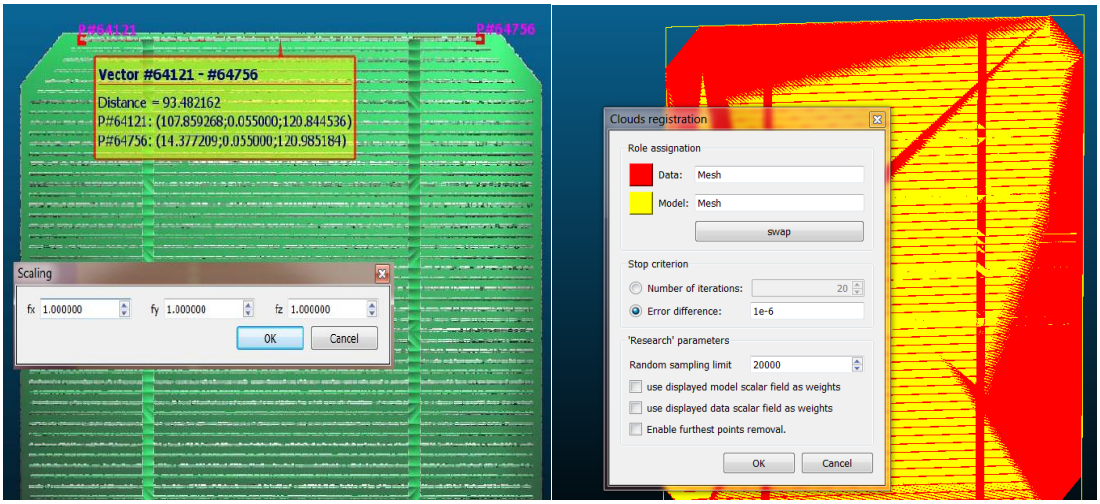

Figure 3.14: Register the two models before 3D measurement. Left - measure the distance between the two specific points in the model and apply the scaling factor. Right - use the Iterative Closest Point (ICP) algorithm to precisely register and finish the superimposition the two models.

The default approach to compute distances between two point clouds is the “nearest neighbor distance”. For each point of the compared cloud, the API searches the nearest point in the reference cloud and computes their (Euclidean) distance. If the reference point cloud is dense enough, approximating the distance from the compared cloud to the underlying surface represented by the reference cloud is acceptable. On the other hand, if the reference cloud is not dense enough, the nearest neighbor distance is sometimes not precise enough. Therefore, the 3D measurement API takes an intermediate way to get a better approximation of the true distance to the reference surface. When the nearest point in the reference cloud is determined, the idea is to locally model the reference cloud surface by fitting a mathematical model, e.g. Delaunay triangulation, on the 'nearest' point and several of its neighbors. The distance from each point of the compared cloud to its nearest point in the reference cloud is replaced by the distance to this model (see Figure 3.15). This is statistically more precise and less dependent on the cloud sampling.

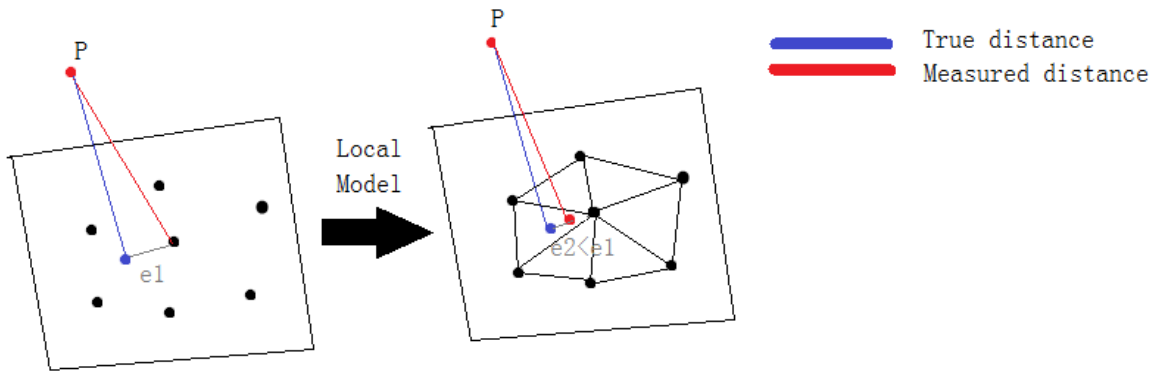

Figure 3.15: Compute distances between two point clouds using local model.

Chapter 4

CASE STUDY: SOLAR CELLS E-QUALITY CONTROL

To demonstrate the proposed methodologies for E-quality control in an industrial setup, solar cells that contain stains, cracks and scratches are used for testing. The testing for the solar modules is very important to understand the real behavior in real weather conditions, although this way we can improve their reliability and efficiency, this by reducing the defects and trying to understand what actions cause the quality problems.

4.1 Design of experiments

This simple experiment proves how a certain percentage of damage in a solar cell or solar panel affects the final efficiency of the solar panel. The experiment consists on measure several panel with different kinds of defects to try to make a relation between the percentage of damage on the panel or cell and the output efficiency of the one. For this experiment we use the same kind and model of solar cells, so the final measurements can be reliable and with this get a solid conclusion.

We measure a very good solar cell, free of defects at first, so that with this we can have a point of comparison. We assume that this cell is 100% efficient, because we are going to compare this one with the defect ones. Then we follow testing process as shown in the Figure 6 below.

Finally, with the final data, we calculate the efficiency for each one of the tested cells, and we make the relationship between the final efficiency and the percentage of damage that the cell presents at the moment of the test.

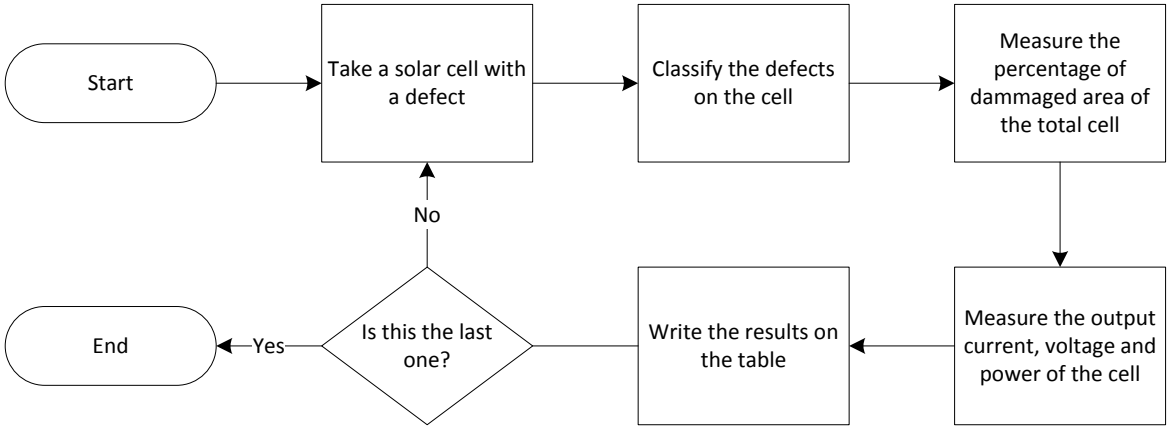

Figure 4.1: The flow chart of the solar panel efficiency test

4.2 Measuring Equipment

We calculate the efficiency for each one of the tested cells, and we make the relationship between the final efficiency and the percentage of damage that the cell presents at the moment of the test. We use a simple circuit to test the efficiency of the solar cells. The diagram of the circuit is presented in Figure 7, including a simple VDC power instead of the solar panel, one resistance of 1K, three LED's and a several resistances of 20K.

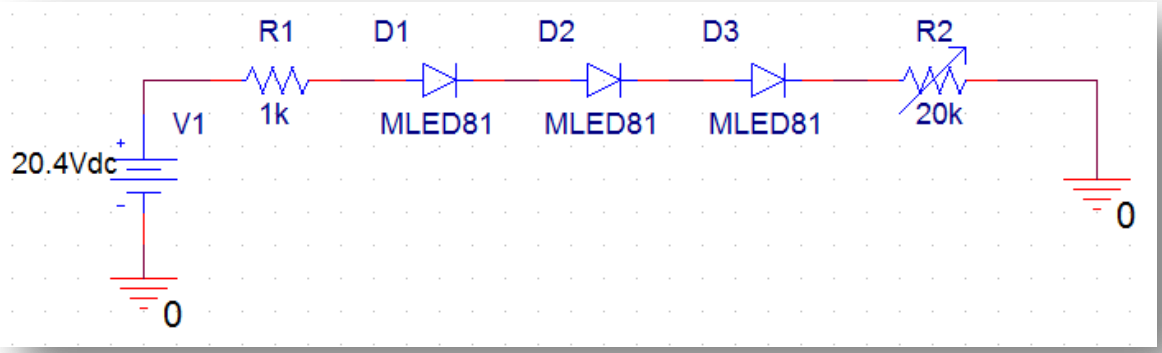

Figure 4.2: Circuit diagram for the solar panel test.3 Classification Analysis

4.3 Analysis

A total of 126 sample solar cells, which have defects such as stains, cracks and scratches, are collected and tested. The results of the solar cell efficiency test are reported in Table 1, and then the solar cells are classified by two systems: the 2D Machine Vision System and the proposed 3D Quality Control System, and then the classification results are compared with each other.

Table 4.1: Results of the solar panel efficiency test. (Where V=Volts, I=Current in mili-amperes, R= resistance in KΩ(kilo ohms), W= Power in watts)

% Damage	V	I	R	W	% Effectiveness
<1	20.4	210	21	4.28	100%
1 ~ 5	20.27	182.2	21	3.69	86.21%

6 ~ 10	20.12	154.34	21	3.11	72.49%
11 ~ 20	19.98	127.54	21	2.55	59.48%
21 ~ 30	19.56	52.68	21	1.03	24.05%
31 ~ 40	18.81	28.91	21	0.54	12.69%
41 ~ 60	18.05	11.66	21	0.21	4.91%
61 ~70	16.2	5.27	21	0.09	1.99%
>75	14.1	0.75	21	0.01	0.25%

From Table 4.1, we can see that solar cells with less than 85% of effectiveness couldn't meet the industry standard and needed to be rejected from the production line. Therefore we make the threshold for the classification of the solar cells as follows:

- Solar cells with more than or equal to 4% of damaged area are classified as Fail
- Solar cells with less than 4% of damaged area are classified as Pass

The following table shows the comparison of the classification analysis using 2D Machine Vision System, 3D Quality Control System and the efficiency test results. From Table 4.2 and Table 4.3, we can see that the 2D Machine Vision System can achieve accuracy of 0.976 and with precision of 0.963 while the 3D Quality Control System can achieve both accuracy and precision of 1compared with the actual efficiency test results.

Table 4.2: The confusion matrix of the 2D Machine Vision System (MVS) classification results

	Predicted	
Actual Efficiency Test	Pass	Fail
Pass	26	2
Fail	1	97

Table 4.3: The confusion matrix of the 3D Quality Control System (QCS) classification results

	Predicted	
Actual Efficiency Test	Pass	Fail
Pass	28	0
Fail	0	98

Table 4.4: Number of cells in each category

Category	A	B	C
# Cells	9	54	17

The Table 4.4 is the summary of the number of cells in each category, in which, cells in category "A" have more than 85% of efficiency, cells in category "B" have between 50% and 85% of efficiency, and cells in category "C" have less than 50%.

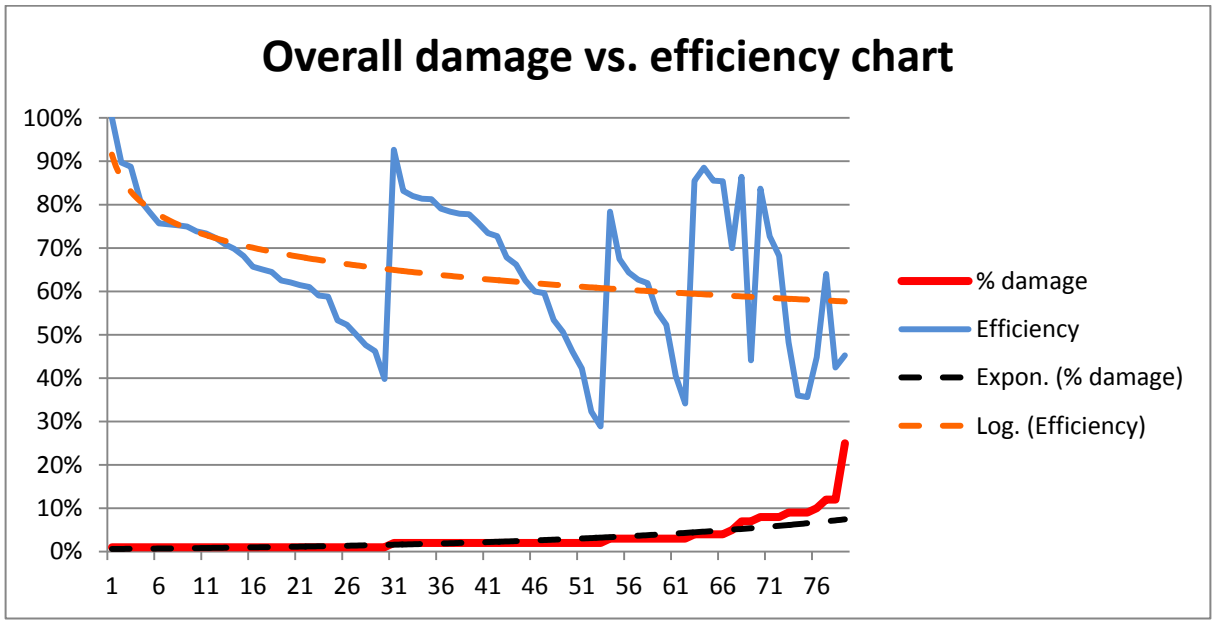

Figure 4.3: Damage % vs Efficiency of the cells

From Figure 4.3, we can see that all the data does not follow a random behavior, this is because we apply a sort pattern following the next rules. First we sort the results by damage %. This is to have a better idea of the distribution of the damaged cells with the same amount of affected area. Next we sort in ascending order the efficiency, we do this because we wanted to see the behavior of the efficiency on the chart vs. the damaged area, but, we do have the randomized data and you can find it in Appendix 1.

Table 4.5: Types of defect

Classification #	Defect
1	Stains
2	Scratches
3	Breaks
4	Cracks
5	Holes
6	Cosmetic defects

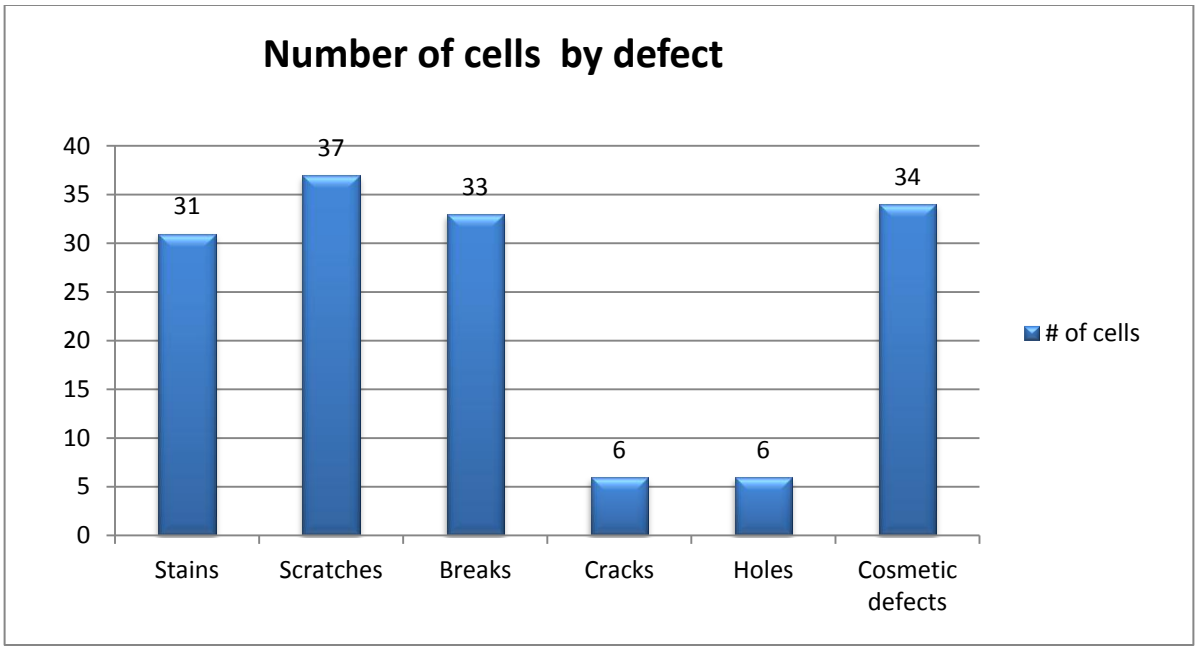

Figure 4.4: Number of cells by defect

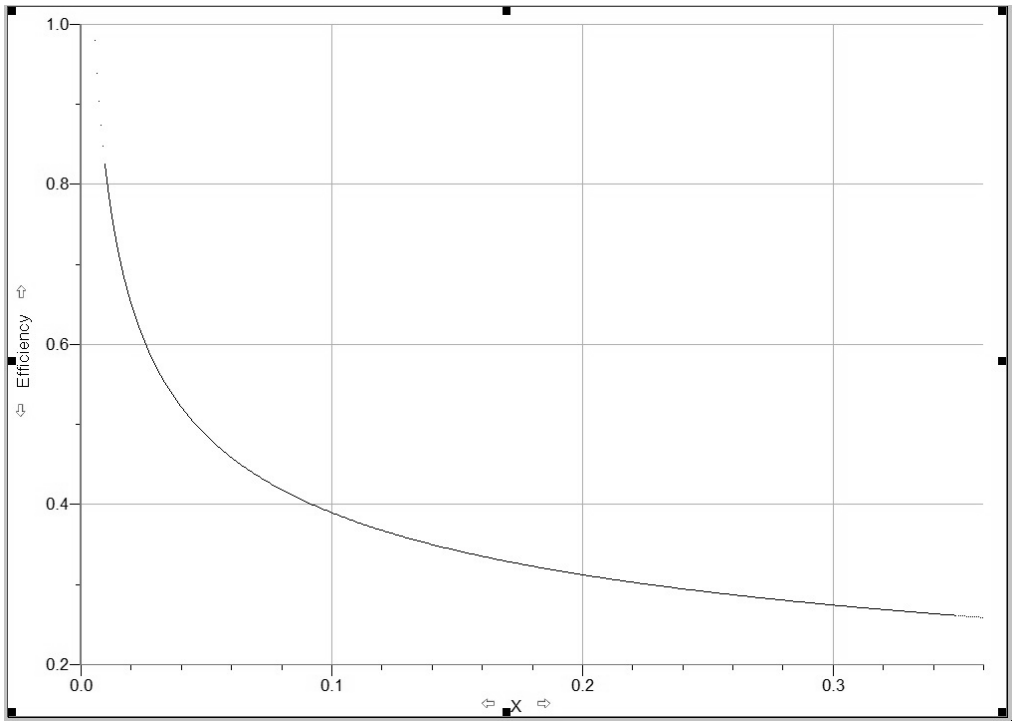

Figure 4.5: Efficiency of solar cells(Y axe) VS. Area of Damage (X axe).

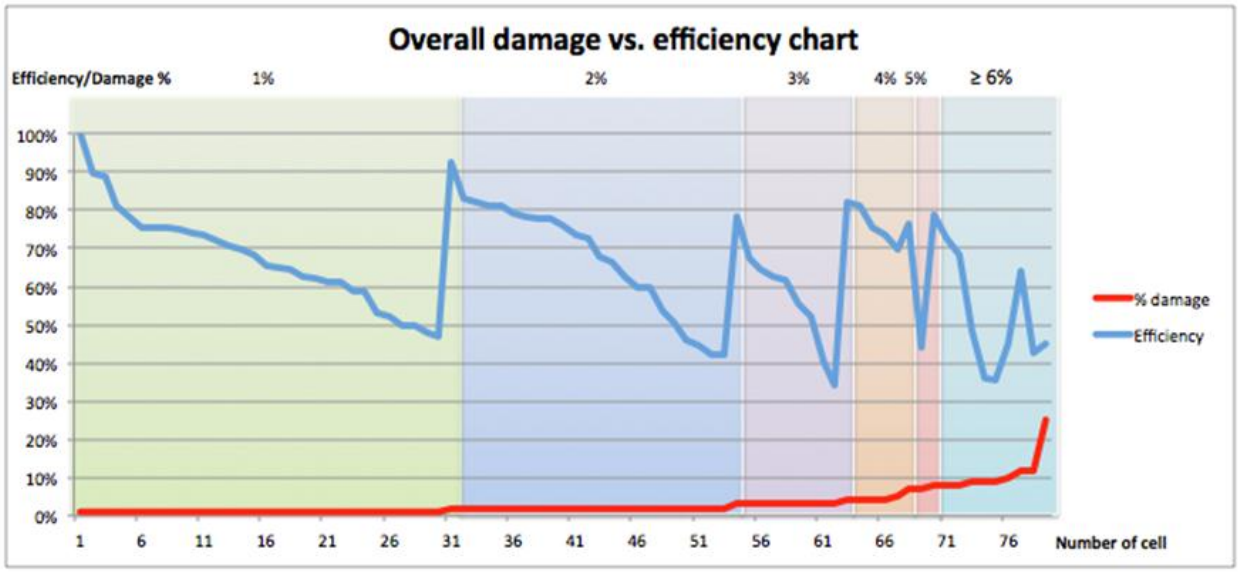

Figure 4.6: Percentage of damage VS. Output efficiency of the solar cells

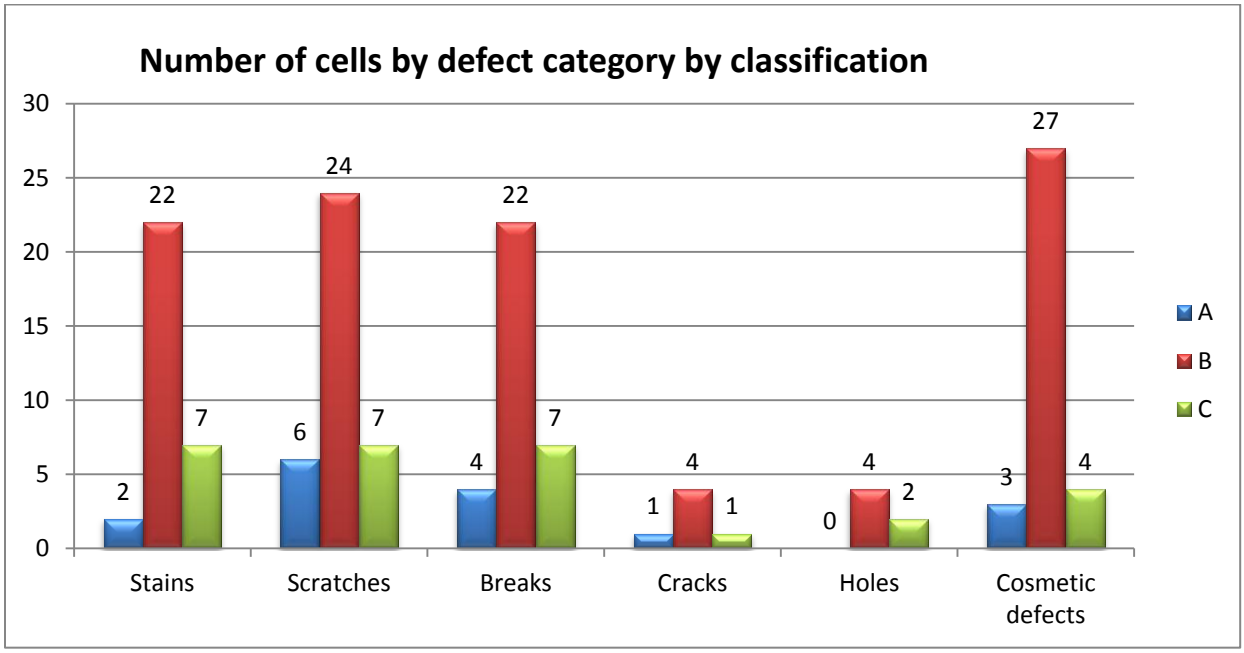

Figure 4.7: Type of cells by defect category

From Figure 4.7, we are watching the number of damaged cells in our 6 defect category groups, and on each category we can see the number of cells by classification, this is “A” for the cells

with more than 85% of output efficiency, “B” for the cells between 50% and 84% of efficiency and “C” for the cells with less than 49% of output efficiency.

Table 4.6: Number of cells and average output efficiency by damage %

Damage %	Number of cells	Averg. Efficiency
1%	30	66.3%
2%	23	66.3%
3%	9	57.4%
> 4%	18	63.9%

As observed inn Figure 4.4, 4.5, 4.6, and 4.7, category 3 or breaks in the solar cells is the one that affects the most the output efficiency of the cells. In table 4.6 we can see that 3% damage has less average output efficiency that 4% or more, and this is because most of the 3% damage cells have the category 3 damage (breaks). Also if we watch the overall results, if we compare the cell with more output efficiency with the cell with more output efficiency of each one of the other categories, the category 3 cell is the one with less efficiency. We can notice also that category 2 (scratches) is the less significant one in terms of output efficiency because is the one with higher overall output efficiency.

Chapter 5

CASE STUDY: PLASTIC INJECTION E-QUALITY CONTROL

The present case study refers to the occurrence of two common defects with plastic injection final parts and the change on dimensions after plastic injection. Plastic injection defects can lead to weakness and even failure by not accomplishing the minimum strength requirements. These requirements may be accomplished but in case aesthetic appearance becomes a main requirement, it may be affected by such defects. Shrinkage is an important aspect to consider during plastic injection due to its importance for the good fit and function of final products. Final inspection for this process consists of visual and first article inspection performed by the operator in charge. Coordinate Measurement Machines may also be used to assure dimension accuracy to final product. If defects are found, if possible, parts may be manually fixed, or in case it is not possible to fix it will be sent to scrap. Defects may happened randomly due to many factors, or they may occur concurrently, and need to be checked to make sure there is no other issues either with the mold, molding process, or materials being used. If dimensional accuracy is not accomplished, parts are simply scrapped.

Plastic injection has become a very useful technology for various industries like automotive, aerospace, and others. Molds are created with metal materials, usually either steel or aluminum, depending on material properties and specifications. When designing a part for plastic injection, it must be very carefully engineered to facilitate the injection and de-molding process. Part small and delicate features, material of the mold, material to be injected, capacity of the molding machine, are some of the important points to take into account when using this process.

These are some critical factors during injection molding (Figure 5.1):

- Temperatures (plastic melting, barrel, nozzle and mold)
- Plastic flow rate
- Plastic pressure
- Plastic cooling time and rate

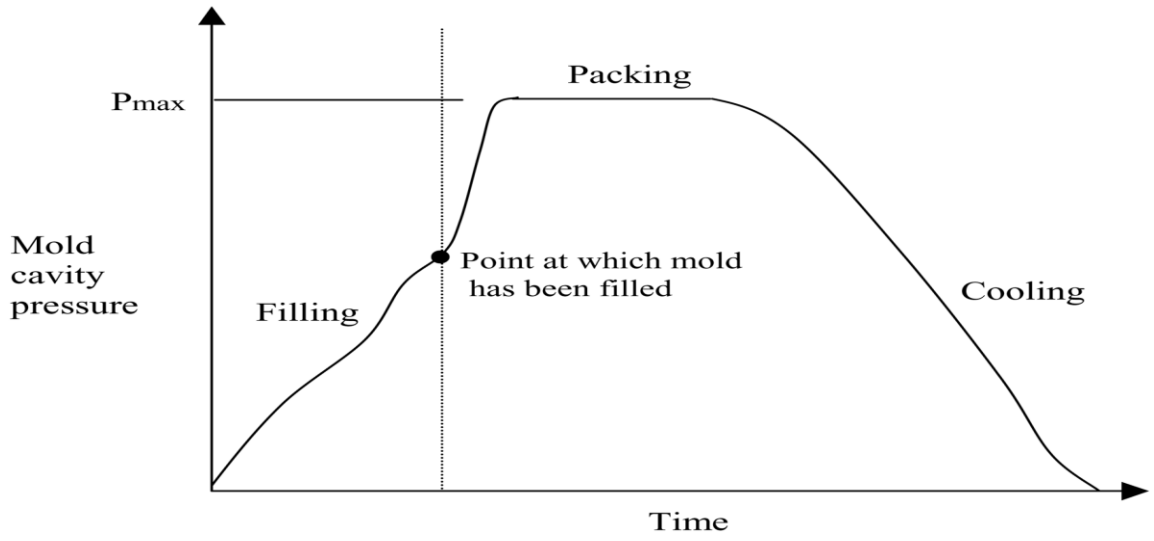

Figure 5.1: Critical factors during injection molding

When a part is manufactured this way, there are several defects that may come up during the process. At this point all employees involved in the process are trained to spot these issues. This means that quality control is dependent on a human being been able to identify such defects. Depending on the defect, the part may not meet its requirements and may not function as it was intended for. There may be little details easily fixable, but there may be other that will not work at all.

Some of the cosmetic defects may include bubbles, cracking, discoloration, flashing, gouge, haze, scratching, among others.

We will be focusing on 2 of these cosmetic defects: flashing and short shots (Figure 5.2).

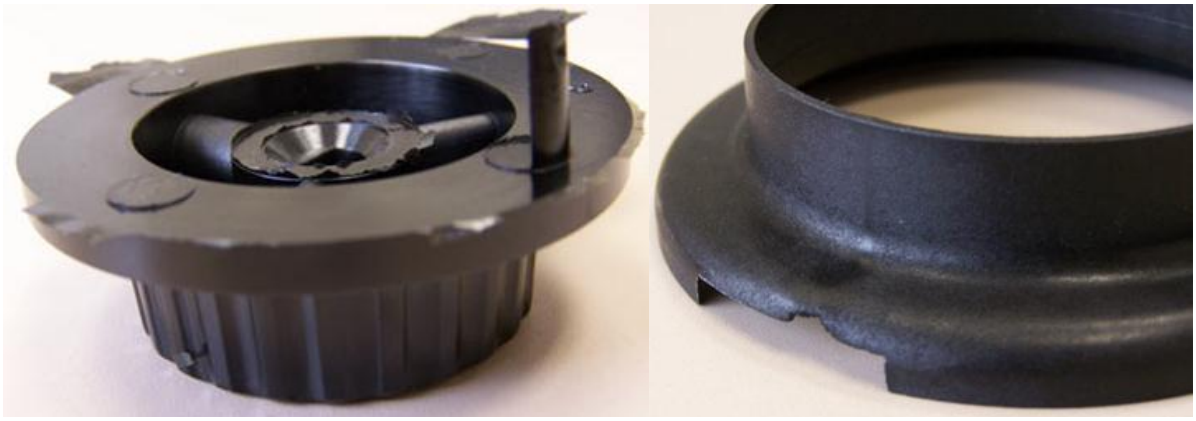

Flashing Short Shot

Figure 5.2 Cosmetic defects: flashing and short shots

Flashing occurs when there is a gap big enough for molten plastic to leak out of the cavity through the line of intersection between two halves of the mold. There are certain specifications that could be follow to avoid this imperfection, but most of the thermoset materials used in plastic injection will flash regardless of press and mold. Short shots refer to the situation when there is too little molten material been injected into the mold and the cavity does not fill properly.

Rejected injection molded parts may cost a lot of money if there is not a good quality control plan established and if personnel don't have the right training to be able to capture defective parts on time. It is required to find any defects before shipping or using injected parts to be able to fix, rework, or simply scrap them.

There are certain points that need to be clarified to solve the problem of surface finish [33]. First there should be an examination of the precise location of the defect and find out when it actually

was evident. Then we need to specify if the defect occurs with every shot or irregularly, if it is always on the same cavity or at the same place in the molding, if we can predict the defect and if it only happens with one machine or others. If we are capable to identify defects on time, we can make sure the proper measurements are taken to avoid major losses due to the lack of information.

To demonstrate the proposed methodologies for E-quality control in an industrial setup, automotive brake calipers that contain different types of defects are used for testing. This part requires certain specifications for color, size, durability, and if these specifications are not met part needs to be scrapped. If part is undersize, it will not fit properly and will cause problems. In the other hand, if it fits perfectly fine but the color is not the specified, it will work just fine but the appearance of the car interior will not be appropriate. It all depends on what kind of defect the part has to determine if it is usable or not.

5.1 Design of experiments

Six key dimensions: diameters of the two circles (D1, D2, D3, D4), and horizontal center-center distance between the circles (CCL1, CCL2), are shown in Figure 5.3. These pieces are machined with a +/- 0.25 mm tolerance limit. Pieces whose dimensions lay outside this range are rejected. Green surfaces are critical since it is in contact with breaking pad.

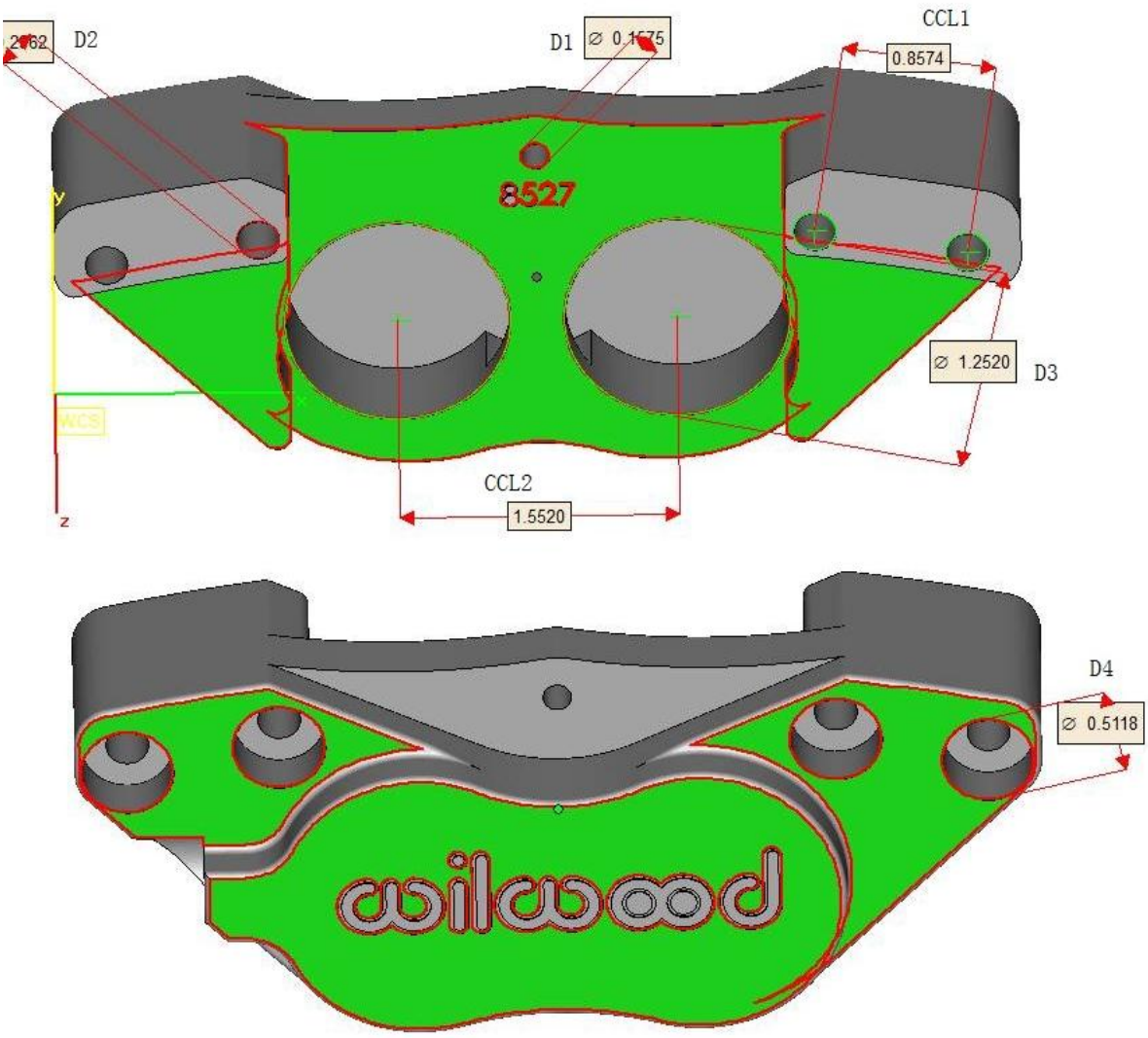

Figure 5.3: Six key dimensions for brake caliper quality control.

Twenty five pieces are made, with a few purposely machined out of tolerance limits on each dimension. Several pieces from each type are mixed up and fed through the conveyor belt for inspection. The flowchart for the testing is shown in the Figure 5.4 below. Although this object does not pose any serious measurement challenge, it presents a moderate complexity for the requirement of our work.

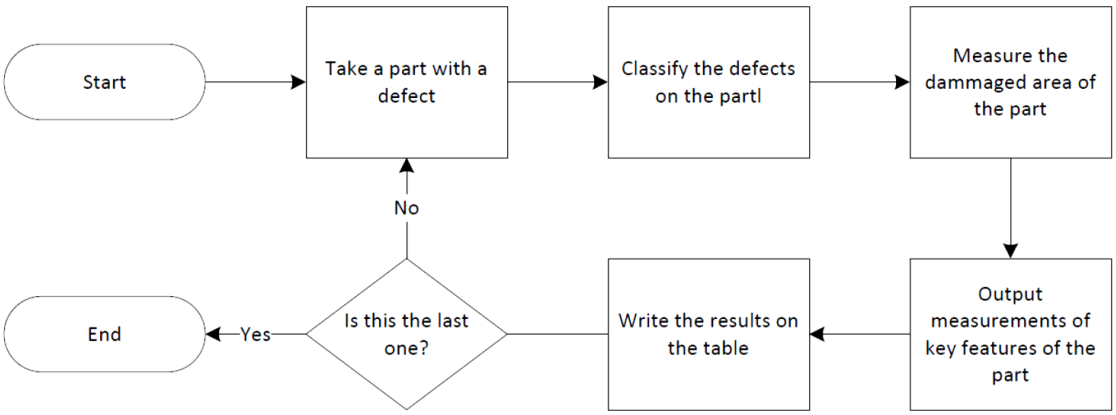

Figure 5.4: The flow chart of the automotive parts quality control

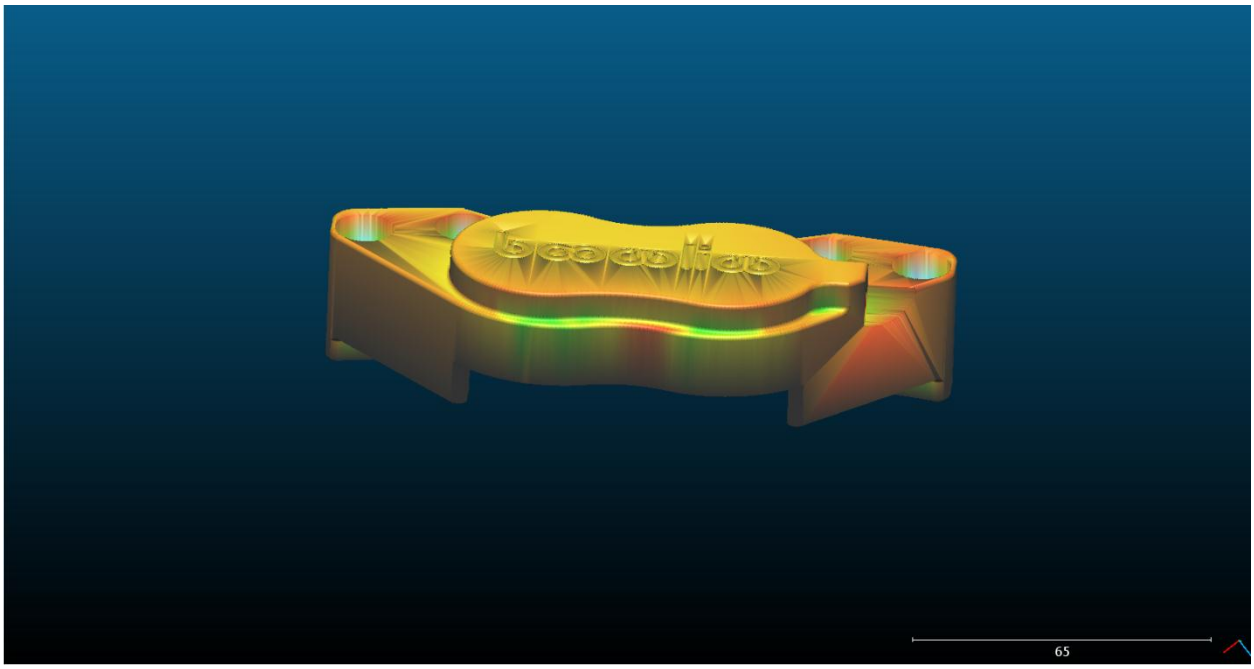

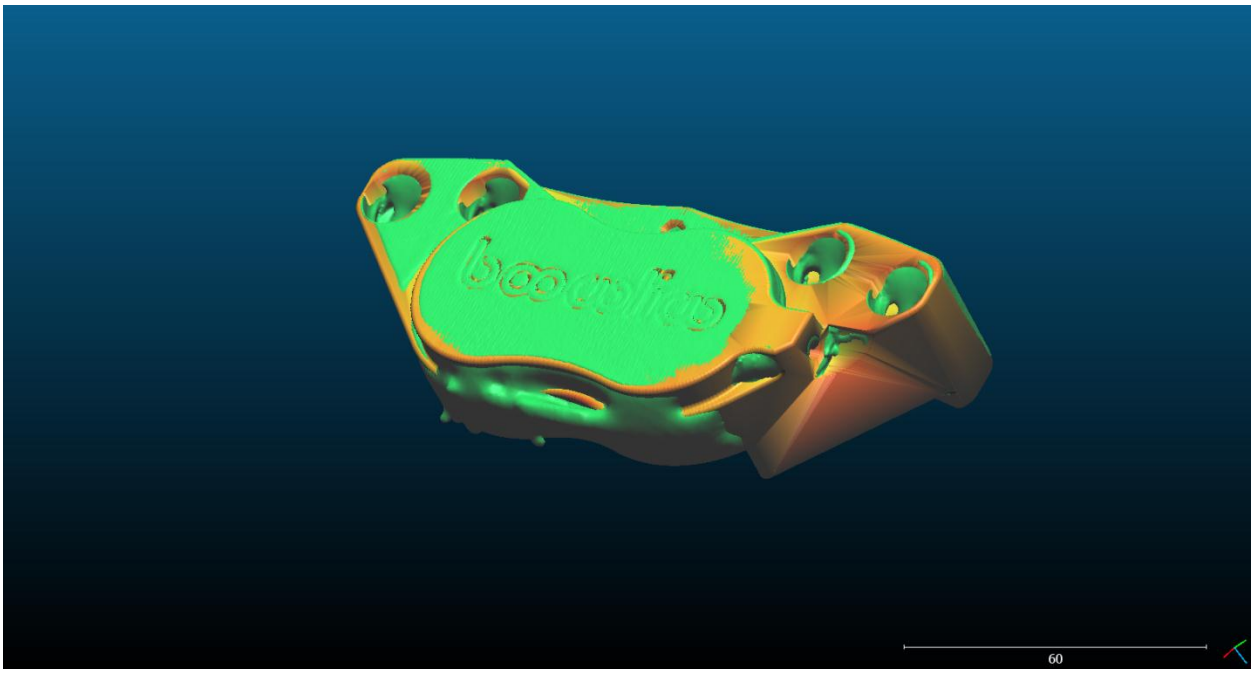

Figure 5.5: 3D Measurement

5.2 Analysis

The outcome of the 3D E-qualtiy control is shown in Table 5.1. Each row stands for a feature measured on parts. Depending on the feature types, it is programmed to automatically classify the features into Pass or Fail status. The user needs to enter the Upper Tolerance Limit (UTL) and Lower Tolerance Limit (LTL) for all features. The measured values are output in the third column. The remaining process is done automatically, and the final result is displayed. With 3D E-qualtiy control, all 25 parts are predicted correctly, resulting in 100% classification accuracy. Table 5.3 shows the prediction result of the brake caliper.

Table 5.1: Prediction outcome of six key dimensions for brake caliper

Key dimensions	Results	Output Value
D1	Pass	0.1575
D2	Pass	0.2662
D3	Pass	1.252
D4	Pass	0.5118
CCL1	Pass	0.8574
CCL2	Pass	1.552

The following table shows the comparison of the classification analysis using 2D Machine Vision System, 3D Quality Control System and the efficiency test results. From Table 5.2 and Table 5.3, we can see that the 2D Machine Vision System can achieve accuracy of 0.88 and with precision of 0.895 while the 3D Quality Control System can achieve both accuracy and precision of 1 compared with the actual efficiency test results.

Table 5.2: The confusion matrix of the 2D Machine Vision System (MVS) classification results

	Predicted	
Actual Efficiency Test	Pass	Fail
Pass	17	2

Fail	1	5

Table 5.3: The confusion matrix of the 3D Quality Control System (QCS) classification results

	Predicted	
Actual Efficiency Test	Pass	Fail
Pass	19	0
Fail	0	6

Chapter 6

CONCLUSIONS

This paper presents a novel 3D E-quality control system that integrates photometric stereo reconstruction for classifying the parts into different categories. This 3D quality control system offers rapid quality control inspection of complex parts while the non-contact photometric scanner provides documented proof that manufacturers are meeting specifications by providing traceable data and accurate 3D models of complex parts, castings, stampings and more. The system captures millions of data points in just minutes to represent the true and full geometry of the complex part. The systems then compare the scanned 3D models to computer aided design (CAD) models to provide accurate and timely measurement feedback for quality control, helping provide proof that the produced products meet the required specification. The data extracted from solar panels was used as case study to demonstrate the proposed methodology. Results show that the new methodology yielded superior results compared to the traditional solar panel inspection approach with very high classification accuracy. The following conclusions were generated from this approach:

(1) Measure the whole part, not just a few points, providing greater assurance that requirements have been met and improving overall quality.

(2) Scan and store 3D models of your complex parts for future viewing, sharing, analysis and measurement.

(3) Create accurate digital models of existing components for re-design or re-engineering purposes.

(4) Help replicate complex parts, tooling or parts that are no longer in production.

Chapter 7

FUTURE RESEARCH

1. In the current work, the proposed methodology was applied to one type of part, developed my mimicking an index part, commonly used in RP industry to benchmark the RP machines. It needs to be tested on wide variety of parts to completely validate the methodology through various types of applications.
2. The proposed procedure of applying 3D measurement for quality control needs further testing to completely validate the results, as the results may vary with different types of defects.

REFERENCES

1. J. Dehmeshki, An adaptive segmentation and 3-D visualisation of the lungs, Pattern Recognition Letters 20 (1999) 919–926.
2. A.C. Jones, A.P. Sheppard, R.M. Sok, C.H. Arns, A. Limaye, H. Averdunk, A. Brandwood, A. Sakellariou, T.J. Senden, B.K. Milthorpe, M.A. Knackstedt, Three-dimensional analysis of cortical bone structure using X-ray micro-computed tomography, Physica A 339 (2004) 25–130.
3. D. Inglis, S. Pietruszczak, Characterization of anisotropy in porous media by means of linear intercept measurements, International Journal of Solids and Structures 40 (2003) 1243–1264.
4. M.F. McNitt-Gray, N. Wyckoff, J.W. Sayre, J.G. Goldin, D.R. Aberle, The effects of co-occurrence matrix based texture parameters on the classification of solitary pulmonary nodules imaged on computed tomography, Computerized Medical Imaging and Graphics 23 (1999) 339–348.
5. C. Vestergaard, S.G. Erbou, T. Thauland, J. Adler-Nissen, P. Berg, Salt distribution in dry-cured ham measured by computed tomography and image analysis, Meat Science 69 (2005) 9–15.
6. S.D. Pandita, I. Verpoest, Prediction of the tensile stiffness of weft knitted fabric composites based on X-ray tomography images, Composites Science and Technology 63 (2003) 311–325.
7. S.F. Nielsen, H.F. Poulsen, F. Beckmann, C. Thorning, J.A. Wert, Measurements of plastic displacement gradient components in three dimensions using marker particles and synchrotron X-ray absorption microtomography, Acta Materialia 51 (2003) 2407–2415.

8. J.F. Delerue, E. Perrier, Z.Y. Yu, B. Velde, New algorithms in 3D image analysis and their application to the measurement of a spatialized pore size distribution in soils, Physics and Chemistry of the Earth (A) 24 (7) (1999) 639–644.
9. Kwon, Y., Chiou, R., Tseng, B. and Wu, T., " Network-based Vision Guidance of Robot for Remote Quality Control," 2010, Robot Vision, Publisher: IN-TECH, Vienna, Austria ISBN 978-953-7619-X-XVenkateswaran, J., and Son, Y., 2005, Production and Distribution Planning for Dynamic Supply Chains Using Multi-resolution Hybrid Models, Simulation (submitted).
10. Chiou, R., Kwon, Y., Tseng, B., Kizirian, R. and Yang, Y.T., "An Internet-based Online 100% Inspection System for Real-Time Robot-Integrated Quality Control," Proceedings of the International Conference on Manufacturing and Engineering Systems (MES 2009), National Formosa University, Taiwan, December 17 - 19, 2009.
11. Tseng, B., Hu, Z. and Chiou, R., "Interactive Remote Control in Internet Based Manufacturing Through YAMAHA Robotic Systems with Webcam," Proceedings of the 14th Annual International Conference on Industrial Engineering Theory, Applications and Practice, Anaheim, CA, October 18-21, pp. 340 – 345, 2009.
12. Chiou, R., Kwon, Y., Tseng, B., Kizirian, R. and Yang, Y.T., "Enhancement of Online Robotics Learning Using Real-Time 3D Visualization Technology," Proceedings of the International Symposium on Engineering Education and Educational Technologies (EEET), Orlando, FL, July 10 - 13, 2009
13. Tseng, B., Aleti, K., Huang, C.C., Ho, J.C., Kwon, Y., Chiou, R. and Sohn, H. "E-Quality Control: A Support Vector Machines Approach," Proceedings of the Industrial Engineering Research 2009 Conference, Miami, FL, May 30 - June 3. 2009.

14. Chiou, R., Kwon, Y. and Tseng, B., "Using Lab VIEW and Network Protocol for Remote Controlling of Closed Loop DC Motor," Proceedings of the Industrial Engineering Research 2009 Conference, Miami, FL, May 30 - June 3. 2009.
15. Pandita, S.D., Verpoest, I., "Prediction of the tensile stiffness of weft knitted fabric composites based on X-ray tomography images," Composites Science and Technology, 63 (2003) 311–325.
16. Dehmeshki, J., "An adaptive segmentation and 3-D visualisation of the lungs," Pattern Recognition Letters, 20 (1999) 919–926.
17. Woodham, R. J., "Photometric stereo: A reflectance map technique for determining surface orientation from image intensity," Proceedings of SPIE's 22nd Annual Technical Symposium (1978), vol. 155.
18. Georghiades, A., "Recovering 3-D shape and reflectance from a small number of photographs," In Rendering Techniques (2003), pp. 230–240.
19. Hertzmann, A. and Seitz, S., "Shape and materials by example: a photometric stereo approach," Computer Vision and Pattern Recognition, 2003. Proceedings. 2003 IEEE Computer Society Conference on 1 (2003), 533–540, vol.1.
20. Mallick, S. P., Zickler, T. E., Kriegman, D. J., and Belhumeur, P. N., "Beyond lambert: Reconstructing specular surfaces using color," Proceedings of IEEE Conf. Computer Vision and Pattern Recognition (2005).
21. Zickler, T. E., Belhumeur, P. N., and Kriegman, D. J., "Helmholtz stereopsis: Exploiting reciprocity for surface reconstruction.," Int. J. Comput. Vision 49, 2-3 (2002), 215–227.

22. Alldrin, N. and Kriegman, D., “Toward reconstructing surfaces with arbitrary isotropic reflectance: A stratified photometric stereo approach,” Proceedings of the International Conference on Computer Vision (ICCV) (2007), pp. 1–8.
23. Zhai, J., Xu, X., Xie, C., Luo, M., 2004, “Fuzzy control for manufacturing quality based on variable precision rough set,” Intelligent Control and Automation, Vol. 3, pp. 2347-2351.
24. Boo, S. K., Deok, H. C., Sang, C. P., 1999, “Intelligent process control in manufacturing industry with sequential processes,” International Journal of Production Economics, Vol. 60-61, pp. 583-590.
25. Kusiak, A., 2001, “Rough Set Theory: A data mining tool for semiconductor manufacturing,” IEEE Transactions on Electronics Packaging Manufacturing, Vol. 24, No. 1, pp. 44-50.
26. Goldberg, D.E., 1989, Genetic Algorithms in Search, Optimization and Machine Learning. Addison-Wesley, Reading, MA.
27. Knier, Gil. "How do Photovoltaics Work?" NASA. (1/20/2010)
28. http://science.nasa.gov/headlines/y2002/solarcells.htm
29. Nelson, J., 2003, “The Physics of Solar Cells,” Imperial College Press; 1 edition, pp.1-15.
30. Lim, Ho, J., Yang, M., and Kriegman, D., “Passive photometric stereo from motion.” in Proc. IEEE International Conference on Computer Vision, vol. 2, Oct. 2005, pp. 1635–1642.
31. Bernardini, F., Rushmeier, H., Martin, I., Mittleman, J., and Taubin, G., “Building a digital model of michelangelo’s florentine pieta,” IEEE Computer Graphics and Applications, vol. 22, no. 1, pp. 59–67, 2002.

32. Nehab, D., Rusinkiewicz, S., Davis, J., and Ramamoorthi, R., “Efficiently combining positions and normals for precise 3d geometry,” in Proc. of the ACM SIGGRAPH, 2005, pp. 536–543.
33. Wilkinson, R., Poppe , E.A., Leidig, K., and Schirmenr, K., “Engineering Polymers: Top Ten Injection Moulding Problems”, http://www2.dupont.com/Plastics/en_US/assets/downloads/top_tens/topten07.pdf

APPENDIX

Appendix A: Raw and randomized data

Cell #	% damage	V	I (mA)	R	W	Efficiency	Type damage	Category
1	1%	342	16.3	20.5	5.57	78.1%	1,2,6	B
2	2%	335	15.5	20.5	5.19	72.7%	2,3	B
3	8%	360	16.6	20.5	5.98	83.7%	3,4	B
4	1%	311	13.5	20.5	4.20	58.8%	2,6	B
5	9%	278	12.4	20.5	3.45	48.3%	3,5	C
6	2%	237	8.7	20.5	2.06	28.9%	1,3	C
7	3%	309	14.3	20.5	4.42	61.9%	3,6	B
8	1%	248	13.3	20.5	3.30	46.2%	2,4	C
9	1%	319	14.7	20.5	4.69	65.7%	2,4,6	B
10	4%	365	16.7	20.5	6.10	85.4%	3	A
11	1%	338	14.4	20.5	4.87	68.2%	2	B
12	1%	354	17.9	20.5	6.34	88.8%	2,4,6	A
13	2%	378	17.5	20.5	6.62	92.7%	2,3	A
14	1%	340	15.8	20.5	5.37	75.2%	1,6	B

15	1%	256	11.1	20.5	2.84	39.8%	1,2	C
16	1%	310	14.4	20.5	4.46	62.5%	2,5	B
17	3%	313	14.3	20.5	4.48	62.7%	1,3	B
18	1%	342	16.9	20.5	5.78	81.0%	2,4,6	B
19	1%	328	15.2	20.5	4.99	69.8%	3	B
20	4%	374	16.9	20.5	6.32	88.5%	1,2,3	A
21	3%	297	13.3	20.5	3.95	55.3%	3	B
22	1%	320	11.9	20.5	3.81	53.3%	1,2	B
23	1%	218	15.6	20.5	3.40	47.6%	3	C
24	2%	291	13.1	20.5	3.81	53.4%	1,3,6	B
25	2%	325	14.9	20.5	4.84	67.8%	1,3,6	B
26	2%	310	14.4	20.5	4.46	62.5%	2,6	B
27	1%	335	13	20.5	4.36	61.0%	2	B
28	2%	357	16.4	20.5	5.85	82.0%	3	B
29	1%	350	18.3	20.5	6.41	89.7%	1,2	A
30	1%	310	14.3	20.5	4.43	62.1%	2	B

31	9%	238	10.8	20.5	2.57	36.0%	2,6	C
32	8%	337	15.4	20.5	5.19	72.7%	2,6	B
33	2%	352	15.9	20.5	5.60	78.4%	1,2	B
34	1%	343	15.8	20.5	5.42	75.9%	2	B
35	2%	270	12.2	20.5	3.29	46.1%	3,6	C
36	1%	343	15.6	20.5	5.35	74.9%	1,2,6	B
37	25%	267	12.1	20.5	3.23	45.3%	5	C
38	35%	317	14.4	20.5	4.56	63.9%	3,6	B
39	12%	311	14.7	20.5	4.57	64.0%	5,6	B
40	1%	326	16.2	20.5	5.27	73.8%	1,2	B
41	2%	330	16.4	20.5	5.41	75.7%	3,6	B
42	7%	353	17.5	20.5	6.17	86.4%	2,3	A
43	1%	306	14.4	20.5	4.39	61.4%	2,3,6	B
44	10%	256	12.5	20.5	3.20	44.8%	3,5	C
45	2%	226	10.2	20.5	2.31	32.3%	1,2,3	C
46	3%	310	15.5	20.5	4.82	67.4%	3,5,6	B

47	3%	235	12.3	20.5	2.89	40.5%	1,2,6	C
48	1%	319	15.9	20.5	5.06	70.9%	1,2,3	B
49	4%	353	17.3	20.5	6.11	85.5%	2,6	A
50	1%	226	15.8	20.5	3.57	50.0%	1,2	B
51	2%	342	16.5	20.5	5.64	79.1%	2,3	B
52	1%	380	18.8	20.5	7.14	100.0%	6	A
53	2%	334	16.7	20.5	5.56	77.9%	3	B
54	12%	252	12.0	20.5	3.03	42.5%	3	C
55	1%	303	15.2	20.5	4.60	64.5%	2,3	B
56	3%	305	15.1	20.5	4.60	64.4%	3	B
57	1%	328	16.4	20.5	5.39	75.5%	1,3,6	B
58	1%	322	16.1	20.5	5.17	72.4%	1,2,3	B
59	4%	377	16.2	20.5	6.10	85.5%	3,6	A
60	3%	277	13.5	20.5	3.73	52.3%	3,6	B
61	1%	305	12.3	20.5	3.73	52.3%	1,3	B
62	1%	295	15.7	20.5	4.65	65.1%	1,6	B

63	2%	271	13.3	20.5	3.62	50.6%	1,2,6	B
64	2%	326	16.1	20.5	5.24	73.4%	1,3	B
65	2%	291	14.7	20.5	4.28	60.0%	2,6	B
66	3%	227	10.7	20.5	2.44	34.2%	1,2,6	C
67	2%	335	16.6	20.5	5.55	77.8%	2,6	B
68	1%	325	16.1	20.5	5.24	73.4%	1,6	B
69	1%	290	14.5	20.5	4.22	59.0%	1,2	B
70	9%	225	11.3	20.5	2.54	35.6%	1,3	C
71	8%	314	15.5	20.5	4.87	68.2%	3	B
72	2%	346	16.8	20.5	5.81	81.4%	2,6	B
73	2%	347	17.1	20.5	5.94	83.2%	3,6	B
74	2%	246	12.3	20.5	3.02	42.2%	3	C
75	2%	345	16.8	20.5	5.80	81.3%	5,6	B
76	7%	251	12.5	20.5	3.15	44.1%	1,2,3	C
77	5%	319	15.6	20.5	5.00	70.0%	1,3,6	B
78	2%	288	14.8	20.5	4.25	59.6%	2,3	B

79	3%	323	17.3	20.5	5.60	78.4%	1,3	B
80	2%	283	16.7	20.5	4.73	66.2%	1,4	B

Appendix B: Damage percentage distribution and average efficiency

Damage %	Number of cells	Averg. Efficiency
1%	30	67.2%
2%	23	66.3%
3%	9	57.4%
> 4%	18	63.9%

Appendix C: Defect catalog table

Stains	Scratches
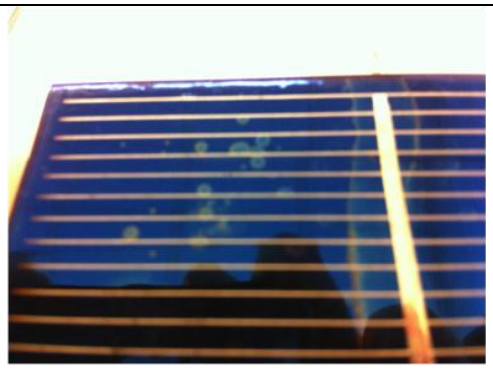	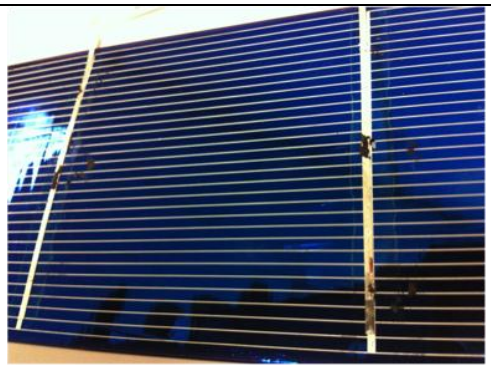
Break	Crack
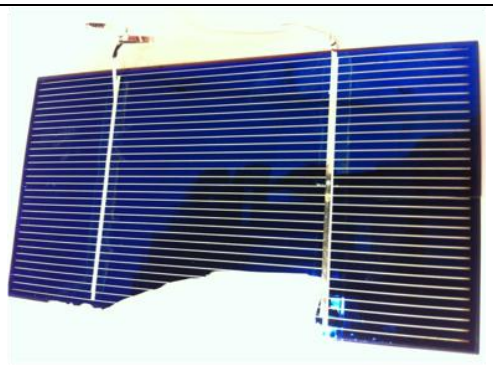	
Hole-Break	Cosmetic defects
	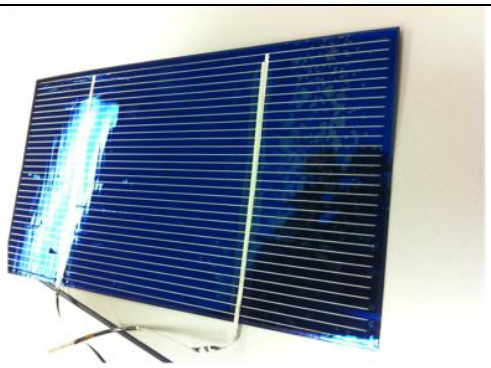
Hole	Scratches

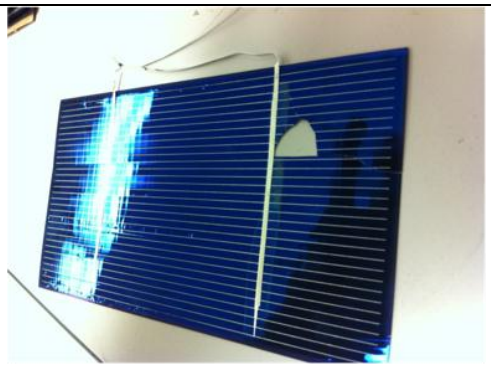	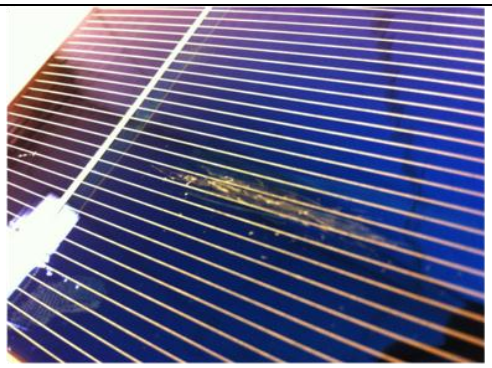
cosmetic defects	crack
	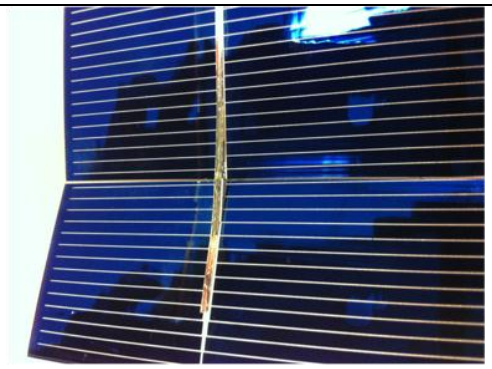
Crack	Break
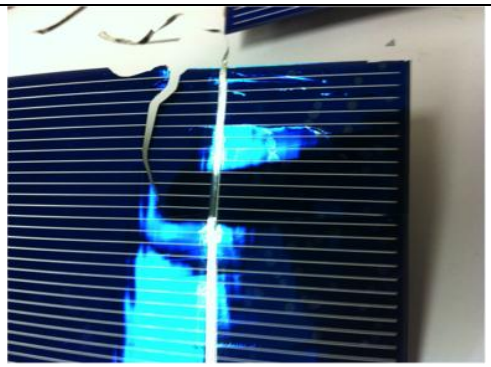	
Cosmetic defects	

	

CURRICULUM VITA

Jun Zheng was born in Hunan, China on October 14, 1981. He graduated from Central South University, China with Bachelor of Technology degree in Electronic Engineering in June, 2004, and Master degree of Signal and Information Processing in June 2007. Then he graduated from The University of Texas at El Paso with Ph.D. degree in Computer Science in December 2010. He started to pursue his Master of Science degree in Industrial Engineering at University of Texas at El Paso from spring 2012. At UTEP, he worked as research assistant at Industrial Systems Engineering Laboratory.

Permanent Address: 14257 Spanish Point Dr. El Paso, TX, 79938

This thesis was typed by Jun Zheng.